The multiphase rheology of magmas from Monte Nuovo (Campi Flegrei, Italy)

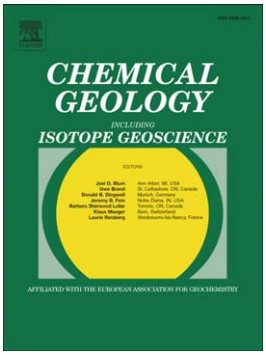

The multiphase rheology of magmas from Monte Nuovo (Campi Flegrei, Italy)

A. Vona, C. Romano, D. Giordano, J.K. Russell

PII: S0009-2541(12)00493-7
DOI: doi: 10.1016/j.chemgeo.2012.10.005
Reference: CHEMGE 16699

To appear in: *Chemical Geology*

Received date: 21 April 2012
Revised date: 28 September 2012
Accepted date: 2 October 2012

Please cite this article as: Vona, A., Romano, C., Giordano, D., Russell, J.K., The multiphase rheology of magmas from Monte Nuovo (Campi Flegrei, Italy), *Chemical Geology* (2012), doi: 10.1016/j.chemgeo.2012.10.005

The multiphase rheology of magmas from Monte Nuovo (Campi Flegrei, Italy)

A. Vona[a], C. Romano[a], D. Giordano[b, c], J.K. Russell[d]

[a] *Dipartimento di Scienze Geologiche, Università degli Studi Roma Tre, L.go San leonardo Murialdo 1, 00146 Rome, Italy*

[b]*Dipartimento di Scienze della Terra, Università degli Studi di Torino, Via Valperga Caluso, 35, 10125 Torino, Italy*

[c]*Institute of Earth Sciences "Jaume Almera", CSIC, Lluis Solé i Sabaris s/n.08028 Barcelona, Spain;*

[d] *Department of Earth and Ocean Sciences, University of British Columbia, Vancouver, British Columbia V6T 1Z4, Canada*

Corresponding author details

phone: +39 06 57338061

fax: +39 06 57338201

e-mail: avona@uniroma3.it

keywords: Campi Flegrei, Monte Nuovo, trachytic magmas, multiphase rheology

9 figures, 5 tables, ca. 13061 words

Abstract

We present a study of high-temperature, uniaxial deformation experiments of natural, partially-crystallized magma from the Monte Nuovo (1538 AD) trachytic eruption. The experiments were performed using a high-temperature uniaxial Geocomp LoadTrac II press at dry atmospheric conditions and under controlled deformation rates. Each experiment involved deforming cores of natural (i.e., crystal- and vesicle-bearing) scoriaceous samples isothermally (600 to 800° C) at constant displacement rates (CDR) corresponding to strain rates between 10^{-7} and 10^{-4} s^{-1}. Measured viscosities vary between 10^{10} and 10^{13} Pa s. The flow behavior of these complex natural materials are fully described by a simplified Herschel-Bulkely equation in terms of consistency *K* and flow index *n*. We estimate the combined effects of crystals and pores on the rheology of these multiphase suspensions. Our results demonstrate that the presence of pores has a major impact on the rheological response of magmas and may produce a marked decrease of their viscosity. At the same time, the presence of pores leads to a strong decrease in the strength of the magma inducing local and temporal variation in the deformation regimes (ductile vs. brittle). Brittle failure was in fact observed at T=600°C and strain rates of 10^{-5} s^{-1} and at T=800°C for the highest applied strain rate (10^{-4} s^{-1}), respectively. This study constitutes an important step toward the estimation of multiphase rheological evolution of Monte Nuovo magmas and toward the general understanding of the full complexities governing the dynamics of magma transport in natural systems.

1. Introduction

The styles, dynamics and intensity of volcanic eruptions are strongly controlled by the properties and behavior of magmas during transport. Consequently, computational models intended to simulate the behavior and hazards of potential eruptions from specific volcanoes depend on detailed, accurate knowledge of the rheology of magmas under volcanic conditions.

Over the past several years, a large number of experimental studies (e.g., Dingwell and Virgo, 1987; Dingwell et al., 1996; Richet et al., 1996; Stevenson et al., 1998; Whittington et al., 2000, 2001; Romano et al., 2001, 2003; Giordano et al., 2004, 2009; Vetere et al., 2007, 2008; Ardia et al., 2008; Misiti et al., 2009) and numerical models (e.g., Russell et al., 2002, 2003; Giordano and Dingwell, 2003; Giordano et al., 2006, 2008; Hui and Zhang, 2007) have improved our understanding of the dependence of silicate liquid viscosity on P-T-X-fO_2. Silicate melts are Newtonian liquids over a wide range of stress and strain rates, and they behave as non-Newtonian fluids only when the shear rate approaches the structural relaxation rate (Webb and Dingwell, 1990a). The viscosity of pure liquids can be calculated to a good approximation as a function of temperature and composition, and may vary by several orders of magnitude for geologically relevant conditions (Giordano et al., 2008).

Natural magmas, however, are commonly transported and erupted at temperatures below their *liquidus*; consequently, they contain suspended crystals and, in the case of near-surface magmas and lavas, bubbles. The presence of suspended solids and bubbles strongly affects the viscosity of magmas and can transform their behavior from simple Newtonian fluids to more complex rheological materials (e.g. Krieger, 1972; Lejeune and Richet, 1995; Bruckner and Deubener, 1997; Deubener and Bruckner, 1997; Manga et al., 1998; Lejeune et al., 1999; Stein and Spera, 2002; Llewellin et al., 2002; Sato, 2005; Caricchi et al., 2007; Lavallée et al., 2007; Cordonnier et al., 2009; Vona et al., 2011). Factors influencing multiphase magma rheology and

eventually the onset of non-Newtonian behavior are the chemical and thermal evolution of the host melt during crystallization and/or bubble segregation, the concentration, shapes, size distributions and maximum packing fraction of suspended particles, as well as the pore fluid pressure and the shear strain rate undergone by magmas.

Moreover, it is known that one major effect of magma degassing is to trigger microlite crystallization due to a sudden increase in the *liquidus* temperature (Sparks and Pinkerton, 1978). By changing the rheological response of the magma, crystallization can, in turn, inhibit bubble growth and bubble coalescence and segregation, hence affecting eruptive styles. This complex interplay between crystallization and bubble segregation indicates that for a full comprehension of magma eruptive dynamics, the combined rheological effects of crystals and bubbles should be both taken into account.

Most rheological studies of natural multiphase suspensions, with few exceptions (e.g., Lavallée et al., 2007; Harris and Allen, 2008; Avard and Whittington, 2012), have focused on the separate effects of crystals and bubbles on magma rheology. These studies have independently modeled crystal-bearing (e.g., Ryerson et al., 1988; Pinkerton and Stevenson, 1992; Pinkerton and Norton, 1995; Sato, 2005; Ishibashi and Sato, 2007; Caricchi et al., 2008; Ishibashi, 2009; Cordonnier et al., 2009; Whittington et al., 2009; Vona et al., 2011) or bubbles/pores-bearing suspensions (e.g., Bagdassarov and Dingwell, 1992, 1993; Stein and Spera, 1992, 2002; Lejeune et al., 1999; Rust and Manga, 2002; Llewellin et al., 2002; Robert et al., 2008a, b).

In this study we use high-temperature deformation experiments to investigate the multiphase (liquid + crystals + bubbles) rheology of natural samples from the Monte Nuovo trachytic eruption (1538 AD, Phlegrean Fields). The 1538 eruption of Monte Nuovo was characterized by two phases with contrasting eruptive styles. The first stage of eruption was characterized by phreato-magmatic activity, generating pumice-bearing pyroclastic density currents and forming a 130-m-high tuff cone (Lower Member deposits). The second phase was characterized

by two discrete Vulcanian explosions whose scoriaceous products were emplaced on the top of the tuff cone (Upper Member deposits, Di Vito et al., 1987; Piochi et al., 2005, 2008; D'Oriano et al., 2005). The second phase was more markedly magmatic and, despite similar chemistry, the textures of the scoria and the micro-crystals content were more variable with respect to the first phase of activity, reaching in some cases 100 vol. % (D'Oriano et al., 2005). These differences in physical properties of magmas are due to different processes occurring during the rise inside the volcanic conduit, and reflect changes in the rheology of the erupted materials.

In order to characterize the rheology of partially crystallized trachytic magmas from the second phase of activity of the 1538 AD Monte Nuovo eruption, we performed a series of controlled deformation rate experiments using an unconfined uniaxial deformation apparatus. The rheological properties of the remelted sample and of melt+crystal mixtures are known from previous studies (e.g., Giordano et al., 2004, 2009; Caricchi et al., 2008). Thus, our experimental data provide a good opportunity to estimate the effects of crystals and vesicles on the rheology of these multiphase suspensions.

2. Rheology of magmatic suspensions

Viscosity is defined as the resistance to flow under specific applied stress (σ) conditions and it is expressed by complex functions of applied stress and resulting strain (ε) and strain-rates (e.g., Herschel and Bulkley, 1926). For a Newtonian liquid, $\sigma = \eta\dot{\varepsilon}$ where η is the Newtonian viscosity. The presence of a solid phase or a gaseous phase to form a solid or bubble suspension can yield non-Newtonian behavior, expressed in the more general equation:

$$\sigma = \sigma_0 + K\dot{\varepsilon}^n \qquad (1)$$

where σ_0 is a stress threshold to be overcome in order to have flow, namely the *yield stress*; *K* is the *flow consistency* (which corresponds to shear viscosity at $\dot{\varepsilon}$ =1 s^{-1}) and *n* is the *flow index* which describes the degree of non-Newtonian behavior, being equal to 1 for Newtonian fluids, *n*>1 for shear-thickening and *n*<1 for shear-thinning fluids. For non-Newtonian fluid, $\sigma/\dot{\varepsilon}$ changes as a function of the deformation rate and if $\sigma_0 = 0$, is equal to $K\dot{\varepsilon}^{n-1}$. In this case, it is convenient to use an apparent viscosity defined as $\eta_{app} = \sigma/\dot{\varepsilon}$ measured at a particular stress or strain rate.

From Eq. (1), assuming zero yield stress (e.g., Lavallée et al., 2007; Avard and Whittington, 2012), the relative viscosity (ratio between stress and strain rate divided by the viscosity of the suspending liquid, η_l) can be written as:

$$\eta_r = \frac{K}{\eta_l}\dot{\varepsilon}^{n-1} \qquad (2)$$

where $K_r = K/\eta_l$ represents the relative consistency.

2.1 Crystal-melt suspensions

A number of experimental and modeling studies have investigated the rheological properties of different crystal-bearing natural magmas at *subliquidus* temperatures (e.g., Shaw, 1969; Gay et al., 1969; Spera et al., 1988; Ryerson et al., 1988; Pinkerton and Stevenson, 1992; Pinkerton and Norton, 1995; Sato, 2005; Ishibashi and Sato, 2007; Caricchi et al., 2008; Ishibashi, 2009; Picard et al., 2011; Vona et al., 2011) or of synthetic silicate suspensions (e.g., Lejeune and

Richet, 1995; Costa, 2005; Caricchi et al., 2007; Costa et al., 2009; Mueller et al., 2010; Cimarelli et al., 2011).

In crystal-melt suspensions, the dispersed phase acts as a 'hard' (non-deformable) inclusion which increases the viscosity of the suspension through both hydrodynamic and mechanical interaction among crystals. For low solid fractions, the viscosity increases slowly with the particle volume fraction (ϕ), and the suspension maintains a Newtonian rheological behavior (strain-rate independent). When ϕ exceeds a critical value (ϕ_c), particles start to interact with each other and a solid network of particles begins to form, causing a strong increase in viscosity and the onset of non-Newtonian flow, characterized by Bingham-like rheology and/or shear thinning effects (Eq. (1)). As the solid fraction is further increased, the system reaches another rheological threshold, corresponding to the maximum packing density of solid particles (ϕ_m), which causes the transition from melt and melt+crystal to solid-state creep rheology (e.g., Kohlstedt and Zimmerman, 1996; Kohlstedt and Holtzman, 2009; Lavallée et al., 2007; 2008; 2012).

The increase in viscosity and the non-Newtonian flow depend on textural features (crystal and bubble distribution) and deformation regimes (e.g., Costa et al., 2009; Petford, 2009; Mueller et al., 2010). Several parameterizations have been proposed to model the effects of crystals on the rheology of suspensions (e.g., Einstein, 1906; Krieger and Dougherty, 1959; Shaw, 1965; Frankel and Acrivos, 1967; McBirney and Murase, 1984; Stickel and Powell, 2005; Costa, 2005; Caricchi et al., 2007; Costa et al., 2009; Ishibashi, 2009; Mueller et al., 2010; Cimarelli et al., 2011; Vona et al., 2011). Costa et al. (2009) proposed an empirical parameterization of relative viscosity as a function of strain rate ($\dot{\varepsilon}$) for low to medium-high concentrated suspensions of spherical particles. Recently, Cimarelli et al. (2011) extended the application of the parameterization to account for bimodal shape polydispersion. The relationships for the variation of the relative viscosity as a function of the solid fraction (ϕ), as used by Costa et al (2009) and Cimarelli et al. (2011), have the following structure:

$$\eta(\phi) = \frac{1+\varphi^{\delta}}{\left[1-F(\varphi,\xi,\gamma)\right]^{B\phi^{*}}} \quad (3)$$

where

$$F = (1-\xi)\,erf\left[\frac{\sqrt{\pi}}{2(1-\xi)}\varphi\left(1+\varphi^{\gamma}\right)\right] \quad (4)$$

with $\varphi = \phi/\phi^{*}$ where ϕ^{*}, ξ, γ and δ are empirical parameters that depend on the deformation rate (Costa et al., 2009; Cimarelli et al., 2011) and B is the Einstein coefficient. This model can successfully predict the multiphase rheology of suspensions varying from ϕ = 0.1 - 0.8 isotropic particles over a wide range of strain rates and includes parameters to account for a bimodal distribution of spheres and elongate crystal of a specific aspect ratio. .

Other authors (e.g Ishibashi, 2009; Mueller et al., 2010; Vona et al., 2011) proposed parameterizations obtained by modifications of the strain rate independent KD equation (Krieger and Dougherty, 1959)

$$\eta_r = \left(1-\frac{\phi}{\phi_m}\right)^{-B\phi_m} \quad (5)$$

to take into account the shear thinning effect on the rheology of suspensions. Ishibashi (2009) provided a modified strain rate dependent KD equation based on rheological measurements on natural basaltic magmas at T from 1177 to 1237 °C:

$$\eta_r = \left(1 - \frac{\phi}{\phi_m}\right)^{-B_1\phi_m[1+\lambda]\ln(1-\phi/\phi_m)\ln\dot{\varepsilon}} \quad (6)$$

where ϕ_m = 0.6 (as in the ER equation), B_1 = 5.46 represents the intrinsic (melt) viscosity at $\dot{\varepsilon}$ =1 s^{-1} and λ = 0.118 is an empirical constant which takes the shear thinning effect into account. However, the fitting parameters are not related to the textural features of the suspensions (e.g., crystal shape, crystal shape dispersion, crystal size dispersion and orientation dispersion), such that the parameterization cannot be applied to other suspensions.

On the basis of their study on monodisperse suspensions with different aspect ratios, Mueller et al. (2010) provided relationships for *K* and *n* as a function of ϕ/ϕ_m and particle aspect ratio (R), respectively:

$$\frac{K}{\eta_l} = \left(1 - \frac{\phi}{\phi_m}\right)^{-2} \quad (7)$$

$$n = 1 - 0.2R\left(\frac{\phi}{\phi_m}\right)^4 \quad (8)$$

where the dependence of the ϕ_m from *R*-parameter is given by:

$$\phi_m = \frac{2}{0.321R + 3.02} \quad (9)$$

With these expressions the relative consistency of monodisperse suspensions is completely described by the Maron-Pierce equation (which correspond to the KD, Eq. (5), with exponent equal to 2; Maron and Pierce, 1956), while the flow index *n* captures the role of shear thinning on the suspension rheology.

Finally Vona et al. (2011) on the basis of rheological measurements on crystallizing polydispersed crystal-rich basalts provided a similar KD-derived parameterization

$$\eta_r = \left(1 - \frac{\phi}{\phi_m}\right)^{-2[1-\alpha \log \dot{\varepsilon}]} \tag{10}$$

in which α is an empirical parameter equal to 0.06 and the effect of crystal shape can be evaluated using the equation proposed by Mueller et al. (2010) (Eq. (9)) to derive the value of ϕ_m, assuming a mean aspect ratio $\bar{R}$ calculated as:

$$\bar{R} = \frac{\sum \phi_i \bar{R}_i}{\phi} \tag{11}$$

where ϕ_i and $\bar{R}_i$ are the crystal fraction and the mean aspect ratio of phase *i*. The model by Vona et al. (2011) is able to describe the rheological behavior of suspensions as a function of strain rate and textural features (i.e., crystal fraction, aspect ratios and shape polydispersion) and can be therefore applied to the complexities of natural magmas.

2.2 Bubble-melt suspensions

The presence of bubbles can either increase or decrease the viscosity of a suspension depending on the dynamic regime (Manga et al., 1998; Stein and Spera, 2002; Llewellin et al., 2002; Rust and Manga, 2002; Llewellin and Manga, 2005). Similarly to solid particles, bubbles deform flow lines within the suspending medium, which tends to increase the viscosity. However, at the same time, they provide free-slip surfaces which favor flow. If the bubbles are spherical, flow-line distortion is great and free-slip surface area is small, hence the overall effect is to increase the suspension viscosity. In contrast elongate bubbles provide small flow-line distortion and great free-slip surface area, yielding a decrease in suspension viscosity (Llewellin and Manga, 2005).

Manga and Loewenberg (2001), Llewellin et al. (2002), Rust and Manga (2002) and Stein and Spera (2002) observed that the viscous regime is controlled by the capillary number Ca, given by:

$$Ca = \frac{\eta_0 r \dot{\varepsilon}}{\Gamma} \tag{12}$$

where r is the undeformed bubble radius and Γ is the bubble–liquid interfacial tension. For Ca<1, interfacial tension forces (which favor sphericity) dominate and bubbles are approximately spherical (e.g., Taylor, 1932). This regime, is usually achieved for small deformation rates and bubble size. For Ca>1, viscous forces (which tend to deform the bubbles) dominate and bubbles will elongate (e.g., Hinch and Acrivos, 1980). These conditions are achieved commonly for high deformation regimes and large bubble diameters.

However, the capillary number implies an equilibrium between viscous and interfacial forces, hence it can be applied only for steady flows, in which the conditions of shear have remained constant for a long enough time to make the bubbles reach their equilibrium shape under

deformation (Llewellin et al., 2002). The timescale over which a bubble can reach this equilibrium shape represents its relaxation time (λ). For a single bubble in an infinite medium this is given by:

$$\lambda = \frac{\eta_0 r}{\Gamma} \tag{13}$$

In steady flow, constant shear conditions must exist for times (t) higher than the relaxation times of the bubble ($t \gg \lambda$). (Llewellin et al., 2002; Rust and Manga, 2002). However, if the shear strain rate is changing, the flow is unsteady. To describe the steadiness of a flow, Llewellin et al. (2002) introduced the dynamic capillary number *Cd*, given by:

$$Cd = \lambda \frac{\ddot{\varepsilon}}{\dot{\varepsilon}} \tag{14}$$

where $\ddot{\varepsilon}$ is the rate of change of strain-rate. For $Cd \ll 1$, the changes in shear environment are slow enough to allow the bubbles to reach their equilibrium shape, hence flow is steady and the dynamic regime is controlled by the capillary number *Ca*. On the other hand, if $Cd \gg 1$, the bubbles are not able to reach their equilibrium shape in response to fast $\ddot{\varepsilon}$, they are therefore unrelaxed (they are actively deforming) and the flow is described as unsteady. In other words, in these conditions the rate of bubble deformation is large compared with the bulk strain rate and, therefore, most of the strain is accommodated by deformation of the gaseous phase. Since the gaseous phase has a negligible viscosity, this leads to a decrease of viscosity as the bubble content increases.

Llewellin and Manga (2005) parameterized the effect of bubbles on the relative viscosity of a bubbly suspension, considering a single equation for the positive dependence of η_r on ϕ and a single equation for the negative dependence of η_r on ϕ, regardless of whether the decrease in

viscosity in the latter case is related to steady (Ca>1) or unsteady (Cd>1) flow. Based on existing literature models, the authors suggested two different parameterizations for each viscous regime (increasing and decreasing η_r), considering two limiting cases corresponding to a minimum and a maximum effect of the bubbles on the viscosity of the suspensions. For Ca<1 (increasing η_r):

$$\eta_r = (1-\phi)^{-1} \quad \text{:MIN} \tag{15}$$

$$\eta_r = 1+9\phi \quad \text{:MAX} \tag{16}$$

from a simplification of Pal (2003) equation (MIN) and Llewellin et al. (2002) (MAX). For Ca>1 or Cd>1 (decreasing η_r):

$$\eta_r = (1-\phi)^{\frac{5}{3}} \quad \text{:MIN} \tag{17}$$

$$\eta_r = \frac{1}{1+22.4\phi} \quad \text{:MAX} \tag{18}$$

from a simplification of Pal (2003) equation (MIN) and Bagdassarov and Dingwell (1992) (MAX).

2.3 Three phase mixtures

Only few studies have explored the rheology of crystal and bubble-bearing magmas. Lavallée et al. (2007), and Avard and Whittington (2012) have investigated natural lavas from domes by uniaxial deformation experiments. The authors have observed pseudo-plastic behavior with a strong shear thinning component for all the investigated magmas and provided equations describing the apparent viscosity as a function of temperature and strain rate for the multiphase magmas.

The individual effect of crystal and bubbles was theoretically parameterized by Phan-Thien and Pham (1997) and later applied by Harris and Allen (2008) for the study of basaltic magmas from

Mauna Loa and Mount Etna. Phan-Thien and Pham (1997) considered three cases as a function of relative size of crystals and bubbles and express the relative viscosity as a function of variable crystal and bubble fraction. In case 1, crystals are smaller than bubbles:

$$\eta_r\left(\phi_{xls},\phi_{bub}\right)=\left[1-\phi_{xls}/\left(1-\phi_{bub}\right)\right]^{-\frac{5}{2}}\left(1-\phi_{bub}\right)^{-1} \quad (19)$$

In case 2, crystals and bubbles are of the same size range

$$\eta_r\left(\phi_{xls},\phi_{bub}\right)=\left[1-\phi_{xls}-\phi_{bub}\right]^{-(5\phi_{xls}+2\phi_{bub})/2(\phi_{xls}+\phi_{bub})} \quad (20)$$

In case 3, crystals are larger than bubbles

$$\eta_r\left(\phi_{xls},\phi_{bub}\right)=\left[1-\phi_{bub}/\left(1-\phi_{xls}\right)\right]^{-1}\left(1-\phi_{xls}\right)^{-\frac{5}{2}} \quad (21)$$

This treatment does not take into account the effect of textural variability, being applicable to spherical particles only, and strain rate dependency on the rheology.

3. Experimental methods

3.1. Sample selection and characterization

Scoriaceous products of 10 to 50 cm in diameter were collected from the so-called Lower Member unit (LM; D'Oriano et al., 2005) and the two sub-units (UM1 and UM2) of the Upper Member (UM), corresponding to the first (LM) and second (UM) stages of activity of the 1538 AD Monte Nuovo eruption, respectively.

The juvenile products from both UM and LM units exhibit very similar K-phonolitic bulk compositions. Groundmass is formed by variable proportions of K-feldspar and glass, with minor sodalite and Fe-Ti oxide in the most crystallized samples. In the LM clasts groundmass, crystal content increases from 13 to 28 vol% from the base to the top of the sequence. Products of the UM consist of clasts with a groundmass crystal content from 30 and 40 vol% to totally crystallized fragments. Crystal size distributions of groundmass feldspars goes from a single population at the base of the Lower Member to a double population in the remaining part of the sequence. Crystal number density increases by two orders of magnitude from the Lower to the Upper Member, suggesting that nucleation dominated during the second phase of the eruption (D'Oriano et al., 2005). Alkali feldspar are generally elongate and have an average aspect ratio of about 1:10. The overall data, morphological, compositional and textural, suggest variations of the magma properties within the conduit.

In order to characterized the samples and to choose the best representative product for rheological characterization, we performed density and vesicularity measurements on both samples from Lower member and Upper Member deposits. Approximately 150 cylindrical cores of 22-26 mm in diameter and 35–50 mm in length were drilled from the Monte Nuovo sample. The measured values of bulk (ρ_B), skeletal (ρ_{sk}) and dense rock equivalent (ρ_{DRE}) densities and the computed values of connected (ϕ_C), total (ϕ_T) and isolated (ϕ_I) porosities are related by formulas provided in Appendix A. All the analyzed specimens showed a bulk density ranging from 1.28-1.64 g/cm^3 (Fig. 1a). Samples from the LM unit showed the lower average density ranging from 1.28-1.51 g/cm^3, compared to sample from the UM unit (UM1 and UM2) ranging from 1.32-1.64 g/cm^3. The dense rock equivalent density (DRE), measured on sample powders, provides a value of 2.65 g/cm^3 and 2.63 g/cm^3 for the LM and the UM units, respectively, in good agreement with values reported by D'Oriano et al. (2005) and Piochi et al. (2005, 2008). From Fig. 1a, we can observe a linear relation between the connected porosity and the skeletal density, which predicts very well our DRE density

measurements. The equivalency of DRE density for both UM and LM products indicates very similar crystal fractions for both investigated samples.

Connected porosity (ϕ_C) ranged from 0.42 to 0.51 for LM samples and from 0.37 to 0.50 for UM samples, while isolated porosity (ϕ_I) is always smaller than 0.02 for both units. Fig. 1b shows the total porosity (ϕ_T) distributions for LM and UM units. Both distributions are unimodal and symmetrical, with the LM sample showing a slight higher mean porosity (as indicated by distributions' peak) and a slight lower dispersion as indicated by its variance $\sigma^2 = 3.2 \times 10^{-4}$ compared to UM curve variance ($\sigma^2 = 7.4 \times 10^{-4}$). The two sets of samples present overall similar absolute porosity and porosity distributions values, and equal DRE. For this, we did not deem necessary to perform rheological investigation on both UM and LM products, and we decided to focus our attention on samples from UM, which is representative of the magmatic phase of activity during the Monte Nuovo eruption and had previously been investigated by Caricchi et al. (2008) in a study on the effect of crystals on magma rheology. The overall crystal fraction determined from image analyses on pre-run samples of UM products is $\phi_{xls} = 0.47 \pm 0.03$ on a vesicle-free basis. Products have a bimodal distribution of sizes ranging from 10 to 200 μm.

The experimental investigations were conducted on eight cores from the Upper Member (UM1) with a variation in total porosity ranging between 0.41 and 0.48 (Table 1). For the deformation experiments, we used samples with aspect ratio close to 2:1 values, an optimum configuration for rock deformation mechanic tests (Mogi, 1966; Hess et al., 2007). The chemical analyses of the UM samples are reported in Table 2. Both bulk rock and matrix glass compositions are trachytic; the glass contains 1.2 ± 0.3 wt.% dissolved H_2O (Caricchi et al. 2008).

3.2. Experiments

Measurements on Monte Nuovo trachytic samples were performed using the parallel-plate method in the volcanology deformation rig (VDR: Quane et al., 2004) at the Volcanology & Petrology Laboratory of the University of British Columbia (Vancouver, Canada) and at the Experimental Volcanology and Petrology Laboratory (EVPLab) of Roma Tre University (Rome, Italy). A detailed description of the VDR is summarized in Appendix B and can also be found in Quane et al. (2004) and Robert et al. (2008a, b). Viscosity calibration using NIST (NBS) standard reference material 717a has evaluated the accuracy of the method to 0.2 log units (Robert et al., 2008a). Prior to deformation experiments, temperature profiles were measured by drilling holes in the center of UM cores and inserting an external thermocouple at different depth throughout their length. A symmetrical gradient of 8-12 °C was obtained across a 4 cm core for the selected insulation setup at T=650 °C after 2 h dwell time (see Quane et al., 2004, and Robert et al., 2008a, for procedure details). This gradient translates to a vertical viscosity change of 0.2 log units, which is within the experimental error of the measurements.

We have calculated the viscosity (η) of the residual liquid matrix (Tab. 2) as a function of temperature and dry conditions using the Vogel-Fulcher-Tammann (VFT) expression [$log\ \eta = A_{VFT}+B_{VFT}/(T-C_{VFT})$] obtained by Giordano et al. (2009), who measured the viscosity of Monte Nuovo magmas. The obtained values of viscosity were used to estimate the characteristic structural relaxation timescales (τ) as the ratio of the interstitial liquid's Newtonian viscosity to bulk shear modulus of silicate melts ($G_\infty=10^{10.5}$ Pa; Whittington et al., 2012), following Maxwell's (1867) relationship (e.g., Dingwell and Webb, 1990). For both hydrous and anhydrous conditions, τ is always < 1 h, over the temperature interval investigated in this study (T=600-800°C; Fig. 2a). The original water content measured in the natural samples varies from 0.9 to 1.5 wt.% (cf. Caricchi et al., 2008). We performed a "zero time" experiment at 600°C and observed, by loss of ignition measurements, that all of the dissolved water is released during the pre-heating and dwell time stages of the experiments (e.g., > 2 hrs at 600-800 °C). Thus, for the purposes of computing the

structural relaxation time and characteristic relaxation rate (Dingwell and Webb, 1990) the melt/glass can be considered anhydrous. Hence we set for each experiment an equilibration dwell time of 2 h after the heating stage in order to allow for thermal equilibration and degassing of the sample. After the beginning of the experiment, an additional 1 h time was allowed for structural relaxation before viscosity determinations.

Uniaxial deformation experiments were performed under isothermal conditions by deforming the crystal- and vesicle-bearing cylindrical specimen at constant displacement rates (CDR). The experiments were carried out at temperatures between 600 and 800 °C and applied strain rates between 10^{-7} and 10^{-4} s^{-1}. Fig. 2b shows the relaxation time (τ) and the characteristic relaxation strain rate ($\dot{\varepsilon}_{relax} = \tau^{-1}$) for the anhydrous Monte Nuovo liquid matrix as a function of temperature. In order to be in the viscous regime at a given temperature, the experimental deformation rate must be slower than the characteristic structural relaxation rate. According to Dingwell and Webb (1990), brittle failure occurs when the applied strain rate ($\dot{\varepsilon}$) is higher than $\dot{\varepsilon} > 0.01\dot{\varepsilon}_{relax}$, and non-Newtonian behavior occurs when it is higher than $\dot{\varepsilon} > 0.001\dot{\varepsilon}_{relax}$. (Dingwell and Webb, 1990; Papale, 1999) (Fig. 2b). Most of the experimental conditions pertain to the Newtonian viscous regime for the liquid matrix (T ≥ 700 °C). Only for the two experiments conducted at 640 °C and 600 °C, the liquids approach the non-Newtonian viscous (T = 640 °C) and brittle (T = 600°C) fields (Fig. 2b).

4. Results

4.1 Rheology

On each measured core of the UM1 subset, from 1 to 7 consecutive segments of deformation were performed at different strain rates. The results of the measurements are reported in Table 3. As an example, Fig. 3a shows the stress – strain paths for experiment runs at T = 750 °C (UM1_E10 and UM1_B14). On sample UM1_B14, three deformation segments (I-III) were conducted at increasing strain rates ($\dot{\varepsilon}_{I-III}$ = 3-10 x 10^{-5} s^{-1}, Table 3). Seven deformation segments (I-VII) were performed on sample UM1_E10, at increasing or decreasing deformation rates ($\dot{\varepsilon}_{I-VII}$ = 0.001-5.3 x 10^{-5} s^{-1}, Table 3). In Fig. 3b, a detail of the first deformation segment on UM1_E10 is shown ($\dot{\varepsilon}_{I}$ = 1 x 10^{-5} s^{-1}). The sample shows an initial increase in stress with increasing strain (and time), followed by flow at constant stress. The apparent viscosity, also shown in Fig. 3b, remains constant during flow of the material.

In order to evaluate the influence of sample heterogeneity on the deformation behavior of the material, we compare in Fig. 3a the stress-strain path of two different cores deformed at T = 750 °C. The sample UM1_B14 shows higher stresses for the same values of strain rate and strain, probably due to a slightly lower initial porosity (Table 3). This difference translates into a viscosity difference of 0.02 $\log_{10}$ units, well within the experimental error. In order to investigate possible strain or time-dependent behaviors, we evaluated the stress response of the material to step-wise increase or decrease of strain rate for sample UM1_E10. From segment I to segment V, at increasing strain, we observed similar stress values for similar strain rates. For instance segment I and IV have similar values of stress and strain rate, but different strains, and the same can be observed for segment II and IV. This indicates that no strain or time-dependent behavior is taking place in this strain-time range. For total strain higher than about 0.13, however, a different behavior is observed. In segment VII, we observe a stress value comparable to segment I and IV, but a lower strain rate (segment VII: $\dot{\varepsilon}_{VII}$ = 3.3 10^{-6} s^{-1}). In this case, we suggest that the increasing strain leads to an accumulation of stress not recovered by the sample which could be associated with a strain

hardening process. The cristallinity was checked by SEM imagin before and after the experiment (Fig. 5). No detectable change in cristallinity was observed for any of the samples. Degassing is completed in the pre-heating stage, as confirmed by "zero time" experiments. Therefore, we suggest that the strain hardening process is related to a strain dependent compaction of the samples, observed by post-run density measurements.

All samples were subjected to different deformation histories, with steps of increasing or decreasing strain rates. All samples, regardless of the deformation paths, reached flow at constant strain rate conditions. Two exceptions are represented by experiment UM1_E4 (run at T = 600 °C the lowest investigated temperature) and by experiment UM1_A12 (T = 800 °C) (Fig. 4). In UM1_E4 (Fig. 4a) brittle failure was achieved at a strain rate of about 10^{-5} s^{-1} and an applied stress of 25 MPa (Table 3), resulting in the failure of the sample. In contrast, the last deformation segment (IV) in experiment UM1_A12 (Fig. 4b) was performed at strain rate of 10^{-4} s^{-1} and lasted until the achievement of a total strain $\varepsilon = 0.43$, much higher than those obtained on the rest of the experimental dataset ($\varepsilon < 0.07$ for each segments). The test showed stress increase up to a peak at 2.86 MPa followed by a continuous decrease with increasing deformation (strain weakening) and a stable value of stress was not achieved.

In the two measurements performed at the lowest strain rate at T = 700 °C and T = 750 °C (UM1_E1B: $\dot{\varepsilon} = 1.1 \times 10^{-7}$ s^{-1}; UM1_E10: $\dot{\varepsilon} = 1.2 \times 10^{-7}$ s^{-1}), the displacement recorded by the device transducer was close to the instrumental resolution (appendix B). As a consequence, the measurements show high signal/noise ratio which translates into large relative errors (>80%) on the strain rate determination. For this reason, those values were discarded.

4.2. Textural and structural analysis of experimental cores

At the end of each measurement, the experimental cores were analyzed to determine the change in core geometry and porosity due to deformation, as illustrated in Appendix A. The results are reported in Table 1. Thin sections of the post-run products were also prepared parallel to the direction of loading to allow for analyses of morphology and features of vesicles and crystals by optical inspection and SEM imaging (Fig. 5a). The crystal content was analyzed prior and after the experiments and no detectable change in crystallinity was observed for any of the sample. In both the pre-run and post-run products, the microlite shape is mostly tabular to acicular. Microlites are generally between 50 to 100 μm long, with average axial ratio 10:1, in agreement with previous studies (D'Oriano et al., 2005; Piochi et al., 2005).

Given the low total strain investigated and the possible small scale heterogeneities of natural samples (pre-run in Fig. 5b; D'Oriano et al., 2005; Piochi et al., 2005), it is difficult to address the contribution of deformation at the microscopic scale. Clear changes in the textural features can only be detected for the high-strain sample run at T=800 °C (UM1_A12, Fig. 5a, c). This sample presents a higher fraction of large vesicles, compared to the non-deformed, indicating a shear induced coalescence. At the macroscopic scale, the large strain may also be responsible for the development of visible fractures (Fig. 5a). Crystal alignment and feldspar microlites curved by flow are also visible (Fig.5c). Curved microlites have been observed also in natural samples by Piochi et al. (2005) who correlates their position along the border of vesicles as an indicator of contemporary growth of microlites and bubbles. In our cases however, curvature of microlite appears to be independent of bubble growth and is possibly related to strain accommodation during deformation.

Fig. 6a shows that the total porosity decreases both in terms of isolated and connected porosity. The effect of deformation on the porosity is quite small, as evidenced by changes of 0-1.5%. The only exception is the high strain experiment UM1_A12, for which a decrease in porosity of about 12% was measured. With this exception, in all other experiments, the total porosity

reduction experienced by our samples is well within the range of porosity distribution of the starting material (Fig. 1). We can conclude that, at the experimental conditions of this study (i.e. low strain), the evolution of porosity with time during deformation remains within values of the natural samples and have a secondary role in determining the rheology of the material.

During uniaxial deformation experiments on porous rocks, strain is manifested by a reduction of sample length (i.e., shortening), a change of core geometry (e.g., barreling),and a reduction of primary porosity (i.e., volume loss). Moreover, the observed reduction of core length, and hence the total strain, can be described by two components: (1) axial strain (ε_a), accommodated by the reduction of sample length; and (2) radial strain (ε_r), accommodated by change of core geometry (e.g., bulging). For low amount of total strain, the volume change can be considered to be accomodated by axial strain mainly due to a decrease in porosity, while the radial strain causes no appreciable volume variation. For these conditions, these components can be calculated independently (Quane et al., 2004; Quane and Russell, 2005; Quane and Russell, 2006). The axial strain is given by:

$$\varepsilon_a = \frac{\phi_i - \phi_f}{1 - \phi_f} \tag{22}$$

where ϕ_i is the initial sample porosity and ϕ_f is the porosity of the run product. Radial strain is given by:

$$\varepsilon_r = 1 - \frac{r_i^2}{r_f^2} \tag{23}$$

where r_i is the pre-run core radius and r_f is the mean radius of the post-run core.

Fig. 6b shows the total sample strain versus the sum of the two independent components (axial and radial). The linear relationship shows that Eqs. (22) and (23) can be used to describe the volume changes related to compression at low strain conditions. However, for high strain ($\varepsilon > 0.4$), the relationship is not consistent anymore, as the volume change is not longer accomodated only by porosity reduction and the radial strain induces volumetric changes. In Fig. 6c the individual contribution of axial and radial strain are compared. For high strain (UM1_A12) however, the increase in the contribution of radial strain (accommodated by core radius increase) is related to microfracturing of the sample which marks the transition from ductile to brittle state.

5. Data Analysis

The flow behavior of natural, partially-crystallized samples from the Monte Nuovo (1538 AD) trachytic eruption was investigated by compression experiments at dry atmospheric conditions and under controlled deformation rates. A variety of rheological responses to deformation was observed, from ductile to brittle behavior as a function of temperature and strain rate conditions. In order to parameterize the flow behavior of these complex natural materials, we consider the stress-strain rate relationships under flow conditions (Fig. 7a). In this figure, data obtained at $\dot{\varepsilon} = 10^{-7}$ s^{-1}, close to the experimental resolution limit, were not included. In general, we observe a linear trend between applied stress and strain rate in the temperature interval investigated, so that at higher applied stresses correspond to higher strain rate values. The measurements at 800 °C show again a log linear correlation, before the onset of strain weakening at $\dot{\varepsilon} = 10^{-4}$ s^{-1}, but they are characterized by a shallower slope.

The effect of strain rate on the apparent viscosity of natural magma from Monte Nuovo is illustrated in Fig. 7b. For all temperatures, the viscosity decreases monotonically with increasing strain rate. A maximum decrease was observed for experiment UM1_E10 run at T = 750 °C where

viscosity at $\dot{\varepsilon} = 10^{-6}$ s^{-1} is 1.1 $\log_{10}$ units higher than at $\dot{\varepsilon} = 5.3 \times 10^{-5}$ s^{-1}. For the purpose of comparison, lines corresponding to the Newtonian viscosity of the suspended liquid calculated after Giordano et al. (2009) for Monte Nuovo total rocks samples, are also shown. At the lowest temperature investigated (T = 640 °C) we observed little or no difference between the liquid viscosity and the crystal- and vesicle-bearing magma. The behaviors start to diverge as the temperature increases, with the multiphase magma showing apparent viscosity higher than the suspending liquid. A maximum difference of 2.62 log units can be observed at the highest temperature (800 °C), translating in a maximum relative viscosity (calculated as the ratio between the measured apparent viscosity, relative to liquid + crystals + pores magma, and the calculated viscosity of the anhydrous liquid).

In the range of deformation rates of this study ($\dot{\varepsilon} = 10^{-6}$ - 10^{-4} s^{-1}) Monte Nuovo magma behaves as a non-Newtonian (shear thinning) fluid at T = 640-750 °C. Only one experiment (UM1_E4) performed at lower temperature (T=600 °C) and $\dot{\varepsilon} = 10^{-5}$ s^{-1}, showed purely brittle behavior. At the highest investigated temperature (T=800 °C), close to the estimated temperature of the Monte Nuovo eruption (850±40 °C, Piochi et al., 2005; Caricchi et al., 2008), the onset of strain weakening (continuous decreasing of stress with increasing deformation) was observed at a strain rate of 10^{-4} s^{-1}. Knowing the onset of strain weakening is very important because it may represent a runaway process during eruptions. Post-run analyses of the sample where strain weakening was observed showed evidence of strain localization, revealed by the preferential alignment of crystals (Fig. 5c). Macroscopic fractures were also observed, indicating that the measurement was performed at the limit between the ductile and brittle fields (e.g., Lavallée et al., 2008).

Caricchi et al. (2008) studied the net effect of crystals on the rheology of non-porous cores of the same Monte Nuovo samples used in this work. Those measurements were performed with a Paterson apparatus, at slightly lower temperatures (T = 550-630°C) and higher strain rates (between 10^{-6} and 4×10^{-4} s^{-1}). The measurements were performed under a confining pressure of 300 MPa,

hence avoiding the loss of the original eruptive H_2O content from the glass (0.86-1.54 wt%). The results of their experiments indicated Newtonian behavior at $\dot{\varepsilon} < 10^{-4}$ s^{-1}, followed by non-Newtonian (shear thinning) and finally brittle behavior at higher shear rates. In our study we never observe Newtonian behavior, even for those measurements performed at similar temperature and strain rate (i.e. UM1_E7; T = 640°C). Possibly, the presence of vesicles could lead to an increase of the T-$\dot{\varepsilon}$ region of shear thinning.

5.2 Fitting of experimental data

The stress – strain rate data obtained at flow conditions and at a constant temperature were firstly fitted using the Herschel-Bulkley model (Eq. (1)). The results of the data fitting are reported in Table 4. Data for strain > 0.15 (UM1_E10-VII and UM1_A12-IV; Figs. 3 and 4), affected by strain dependent rheology (hardening and weakening), were not included. Overfitting with a three-parameter equation lead to very high standard errors. At all temperatures, the calculated values of yield stress σ_0 from the regression approximately equal zero, except for T = 725 °C and T = 750 °C where they equal 0.99 and 0.16 MPa, respectively. Assuming $\sigma_0 = 0$, we have re-fitted the data to the following simplified power law expression (e.g., Lavallée et al., 2007; Avard and Whittington, 2012):

$$\sigma = K\dot{\varepsilon}^n \tag{24}$$

Fitting can be expressed in log terms for stress (Fig. 7a) or for apparent viscosity (Fig. 7b):

$$\log\sigma = \log K + n\log\dot{\varepsilon} \tag{25}$$

$$\log\eta_{app} = \log K + (n-1)\log\dot{\varepsilon} \tag{26}$$

The fitting is good across the whole dataset (R^2 = 0.94-0.98). The results of the fits are reported in Table 4 and in Fig. 8 as a function of temperature. A linear relationship can be observed between flow parameters (*log K* and *n*) and T (Fig. 8). Flow consistencies decrease with increasing temperature from *log K* = 9.60 at T = 640°C to *log K* = 7.67 at 800°C (Fig. 8a). Flow index *n* varies from 0.4 and 0.3 in the temperature interval considered, and a slight decreasing trend can be recognized (Fig. 8b), with the exception of the outlier point at T = 750°C. Simple linear regressions for flow parameters as a function of T yield the following relationships:

$$\log K = 16.722 - 0.0113T \quad (27)$$

$$n = 1.0255 - 0.0009T \quad (28)$$

By substituting Eqs. (27) and (28) into (25) and (26), flow curves and apparent viscosity can be derived for the multiphase Monte Nuovo UM magma as a function of temperature and strain rate. Fig. 8c shows calculated vs. measured apparent viscosities using Eqs. (27-28). Prediction error are below 0.3 log units for shear viscosity obtained with Eqs. (27-28) for all but sample UM1E10 taken at 750°C, which shows a slightly higher deviation (<0.5 log units).

5.2 The combined effect of crystal and pores on the rheology of Monte Nuovo magmas.

The values of relative viscosity (η_r), calculated as the ratio of the measured apparent viscosity (liquid + crystals + pores) and the viscosity of the anhydrous liquid calculated after Giordano et al. (2009) on Monte Nuovo liquids, are reported in Table 3 and plotted in Fig. 9a as a function of temperature. Giordano et al. (2009) measured the viscosity of the Monte Nuovo remelted bulk rock and provided a parameterization for this specific composition. The interstitial

liquid of our samples is slightly more evolved compared to the bulk rock analyzed by Giordano et al. (2009) (Tab. 2). In order to correct for the evolution of the residual liquid, we calculated, based on the GRD model (Giordano et al., 2008) the viscosity of the bulk matrix and of the residual liquid and a difference of about 0.2 log units was derived at all temperatures. We corrected the liquid viscosities for this value and calculated the relative viscosity accordingly.

From the Fig. 9a, it is apparent that crystals and vesicles increase the viscosity of the magma, with respect to that of the interstitial liquid at 700-800 °C and at the investigated strain rates. The amount of increase is clearly a function of applied strain rate (owing the shear thinning behavior) and of temperature. In fact, the maximum increase can be observed at 800 °C where relative viscosities are between $\log_{10}$ 1.50 and $\log_{10}$ 2.39, depending on the applied strain rate, and then it decreases with decreasing temperature. The temperature dependence of the relative viscosity cannot be an artifact of the normalization procedure, as this has been performed on the same melt composition (Monte Nuovo) with respect to that investigated in this study, so other explanations may be invoked to explain this apparent anomaly. A similar behavior was reported by Caricchi et al. (2008) where the highest relative viscosity values were associated with the lowest viscosity of the melt phase. According to the Caricchi et al. (2008), the enhanced rheological difference between crystals (i.e. feldspar, the dominant phase) and interstitial liquid at high temperature may be responsible for the increase of relative viscosity. Given the similarity of the activation energy of liquid and crystals plastic flow at low T (303 and 332±32 KJ/mol at T = 500-600 °C, respectively; Rybacki and Dresen, 2004; Giordano et al., 2009), the authors argued that part of the deformation could be taken up by the suspended crystals. On the contrary, at higher temperatures the difference between the activation energies become more marked and the deformation would be mostly concentrated on the melt phase, hence enhancing the effect of crystals as non-deformable solids increasing the relative viscosity. Alternatively, the presence of bubbles could generate this

temperature dependence. At this stage, it is difficult to separate these effects and further discussion would be too speculative.

At T = 640 °C we obtain a relative viscosity value lower than unity ($\log_{10} \eta_r = 0.3 \pm 0.1$) (i.e. the viscosity of the suspension is approximately the same as the viscosity of the interstitial liquid). At T = 640 °C, the conditions of suspension deformation overlap with the glass transition interval (T_g = 630-650 °C) based on calorimetric measurements at cooling rate between 5-20 °K/min (Giordano et al., 2005). If the glass transition region is reached, the applied stress could be essentially accommodated by brittle failure, lowering the relative viscosity values. However, no induced fractures were recognized from the post run textural analysis, probably due to the small amount of strain suffered by the sample ($\varepsilon_m < 0.06$). As shown in Fig. 2b, even if the glass transition is not crossed, at T = 640 °C and at the applied strain rates ($\dot{\varepsilon}$ = 3-6 x 10^{-6} s^{-1}), the suspension may be approaching the non-Newtonian field. In this case, a liquid viscosity lower than that calculated from Giordano et al (2009) would be expected due to liquid shear thinning (Dingwell and Webb, 1990), resulting in relative viscosities greater than those shown in Fig. 9. For these reasons, data at T = 640°C should be treated cautiously.

In Fig. 9b, the relative viscosity of the multiphase suspension is shown as a function of crystal fraction and strain rate. The crystal fraction ϕ_{xls} is equal to 0.47 ± 0.03, calculated with respect to the solid fraction from SEM image analyses. The effective crystal content is then obtained by sample porosity as: $\phi_{xls*} = \phi_{xls}(1- \phi_T)$. The variability observed is due to the original porosity hetereogeneity of the samples.

The relative viscosities of two phases crystal bearing suspension calculated after Vona et al (2011) (Eq. 10) are also reported in the Figure, calculated for three different strain rates (10^{-6}, 10^{-5}, 10^{-4} s^{-1}) and a mean crystal aspect ratio of $\bar{R}$ = 10 (D'Oriano et al., 2005).

The Vona et al (2011) parameterization for crystal-bearing suspensions yields values equal or higher compared to our results. From the data in Fig.9b, the decrease in relative viscosity compared to Vona et al. (2011) appears to be related to the presence of pores. Pores/bubbles seems to have a major impact on rheology decreasing relative viscosity of more than one order of magnitude. A quantitative evaluation of the effects of bubbles on the multiphase rheology of Monte Nuovo magma is hampered by the paucity of data and very little exists in the literature regarding the combined effects of bubbles and crystals on the viscosity of magmas. In Fig.9b, we show the only (to our knowledge) theoretical treatment for a three-phase mixtures by Phan-Thien and Pham (1997) (Eq. 19, 20, 21) applicable to a suspension of rigid spheres and bubbles. The three equations differ for the relative sizes of crystals and bubbles. Our results are comprised between the parameterization of Vona et al. (2011) for the effect of crystals only and the parameterization of Phan-Thien and Pham (1997) for the effect of crystals and bubbles, indicating a mixed contribution of the two phases in the viscosity of the magmas. However, Phan-Thien and Pham (1997) treatment does not take strain rate or crystal distribution and shape into account, particularly important in our case given the marked elongation of K-feldspar crystals. Moreover, bubbles are considered spherical and always increasing the viscosity of the liquid, which is not presumably true in our case. Those approximations limit the applicability of this treatment to our magmas or to natural magmas which display different textural features compared to those analyzed in the treatment. Additional studies are necessary to further explore and quantify the multiphase rheology of natural magmas, whose knowledge is of primary importance for our understanding of the dynamic of volcanic processes.

6. Volcanological implications

This investigation has been conducted on natural samples at atmospheric pressure conditions. Therefore, the pores, which are interconnected, are filled with air. In natural pre-eruptive magmatic environments, magma bubbles may be filled with pressurized fluids with a pore pressure equivalent to confining pressure (assuming equilibrium), counteracted by the efficiency of degassing processes. Our investigation, conducted at ambient conditions, is especially applicable to lava flow emplacement and to upper conduit flow where degassing is efficient and permeability is high enough to maintain connected pore pressure close to atmospheric pressure. According to Piochi et al. (2008), the high vesicle connectivity (>95%) associated with the vesicularity ($\phi \sim 0.4$) of material from Monte Nuovo scoriae is characteristic of vesiculation under open-system conditions and efficient outgassing.

In our study, we observe that the presence of suspended crystals and bubbles induces complex rheological behavior. In particular, sample UM1_E4 (T= 600°C) undergoes pure brittle failure at 25 MPa and 10^{-5} s^{-1}. Sample UM1_A12, (T=800°C, $\dot{\varepsilon} = 10^{-4}$ s^{-1}) shows a ductile behavior followed by strain weakening at 2.9 MPa. The ultimate stresses before failure in sample UM1_E4 and before strain weakening in sample UM1_A12 correspond to the uniaxial compression strength of the material. Caricchi et al. (2008) for pore-free Monte Nuovo magmas, reported values of stress at the onset of strain weakening, for comparable strain rates, approximately two orders of magnitude higher (180 MPa at 575 °C to 258 MPa at 630°C) than the measured values in the present work. Extrapolation of their data at 800 °C, yields values of about 900 MPa, much higher than those found in our study. The large difference between the two sets of studies may be due to the presence of pores which decreases substantially the strength of the magma. However, confined pressure and different temperatures could also play an important role.

From fiber elongation studies, Webb and Dingwell (1990b) found that the tensile strength of magmas range from 350 MPa for rhyolitic compositions to approximately 250 MPa for more mafic melts. Similar values have been found in other studies (Romano et al., 1996; Mungall et al.,

1996) and, despite the different experimental conditions, they are in good agreement with the results from Caricchi et al. (2008). In our case, brittle failure occurs at approximately 2 MPa and 800 °C and 25 MPa at 600°C. This extremely low strength is compatible with the behavior observed for vesicle- bearing magmas and glasses at different shear stress-shear strain rate conditions (Romano et al., 1996; Mungall et al., 1996; Stevenson et al., 1998) which was related to the concentration of stress at the vesicle-melt interface which favors brittle failure.

We therefore observe that the presence of pores enhances the fluidity of the magma yet at the same time decreases the strength of magmas and leads to rapid onset of brittle fragmentation. Switching between glassy and liquid behavior may occur during lava flow emplacement of acidic magmas due to local variation in stress conditions (output rates, topography, Tuffen et al., 2003; Gonnermann and Manga, 2005; Dingwell, 2006). According to this mechanism, magma fragments can weld and flow if shear stress decreases or break if the stresses increase. In addition to stress variation, local heterogeneities in the pores/bubble distribution due to variable degassing and crystallization kinetics can lead to regions of flow and/or brittle behavior and temporal crossing of the glass transition, giving rise to morphological heterogeneities observed in many lava flows.

7. Summary

The multiphase rheology of natural vesicle- and crystal- bearing magmas from Monte Nuovo was investigated by uniaxial deformation experiments in the T range 600-800 °C and at strain rates between 10^{-7} and 10^{-4} s^{-1}. Brittle behavior was observed at 600°C and 10^{-5} s^{-1}, and at 800°C and 10^{-4} s^{-1}. All the other experiments were performed in the ductile regime where non-Newtonian shear thinning behavior was observed in the apparent viscosities range of 10^{10}-10^{13}. A parameterization of the flow behavior in terms of consistency *K*, flow index *n* and temperature was

performed. After normalizing the measured multiphase viscosity (liquid+crystal+vesicles) to the calculated viscosity of the suspending liquid, the net combined effect of crystals and pores on the rheology was determined. The relative viscosities displayed a dependence on both experimental temperature and applied strain rate. Higher relative viscosities (up to 2.4 $\log_{10}$ units) were observed with increasing temperature and decreasing strain rates. Relative viscosity values close to unity were observed at T = 640 °C, close to the glass transition temperature (Giordano et al., 2005). The comparison with crystal-bearing models of viscosity (Vona et al., 2011), show that the presence of pores has a major impact on the rheology of magmas and can lead to a decrease of viscosity of more than one order of magnitude. At the same time, the presence of pores leads to a strong decrease in the strength of the magma inducing local and temporal variation in the deformation regimes (ductile vs. brittle) during lava flow emplacement. which may result in the textural heterogeneities (flow banding) observed in many silicic obsidian lava flows.

Acknowledgements

D. Giordano acknowledges support from the Subdirección General de Formación e Incorporación de Investigadores – Programa Ramón y Cajal (RYC-MICINN) del Ministerio de Ciencia y Innovación – Dirección General de Investigación y Gestión del Plan Nacional de I+D+i (DGI) de España.

Appendix A. Pre- and Post-experimental sample characterization.

Volcanic rocks contain two types of porosity: connected and isolated. Connected is defined as the volume fraction of pores that are connected to each other and can be physically accessed by gas or fluid. Isolated porosity is defined as the volume fraction of porosity that is isolated by the

skeletal framework. The total porosity of a rock (ϕ_T) is given by the sum of connected and isolated porosities and is:

$$\phi_T = \frac{V_{\phi_T}}{\left(V_{DRE} + V_{\phi_T}\right)} \quad \text{(A.1)}$$

where V_{DRE} is volume of the dense rock equivalent (e.g., powder) and $V_{\Phi T}$ is the volume of the total pore space in the sample. Connected (ϕ_C) and isolated (ϕ_I) porosities are given by:

$$\phi_C = \frac{V_{\phi_C}}{\left(V_{DRE} + V_{\phi_C} + V_{\phi_I}\right)} \quad \text{(A.2)}$$

$$\phi_I = \frac{V_{\phi_I}}{\left(V_{DRE} + V_{\phi_I}\right)} \quad \text{(A.3)}$$

The corresponding densities are defined on the basis of how they are measured. The dense rock equivalent (DRE) density of the sample (ρ_{DRE}) is the density of the rock framework of the sample alone (e.g., no porosity) and was measured on samples of rock powder by He-pycnometry. Powdering the sample ensures that there are no pores and that the He-pycnometry experiment measures the true volume (V_{DRE}) of a fixed mass of rock powder (M_R).

$$\rho_{DRE} = \frac{M_R}{V_{DRE}} \quad \text{(A.4)}$$

The skeletal density (ρ_{sk}) is the density of the rock and the isolated porosity. Using He-pycnometry, the gas infiltrates the samples connected pores but cannot access the isolated pores. Therefore, the He-pycnometry experiment measures the volume of the rock/solid framework and the isolated (inaccessible) pores (e.g., the skeletal volume: $V_{DRE} + V_{\phi I}$).

$$\rho_{sk} = \frac{M_R}{\left(V_{DRE} + V_{\phi_I}\right)} \tag{A.5}$$

For pre-run samples, the bulk density (ρ_B) was measured on cylindrical cores of rock samples using the mass (M_R) and a bulk volume estimated from the geometry of the core ($\pi*L*r^2$), from the averages of replicate measurements of diameter and length. For post-run cores, which underwent compression and bulging or failure, the bulk volume was determined by two methods: (1) archimedean buoyancy on the samples coated with paraffin and (2) image analysis measurements on thin sections cut through planes parallel to the direction of loading. In the first case, the paraffin coatings were performed by immersing the sample in a bath of liquid paraffin (T = 100 °C). Samples were weighed before and after the paraffin coating, in order to calculate the mass of the applied paraffin. The paraffin density (0.834 g/cm^3) was used to extract the bulk volume of the samples. In the second case, the post run length was measured directly on scaled scanned images of the thin section (Fig. 5a) and an average (equivalent) final radius was obtained by the ratio between the two-dimensional area and the length. The two methods gave similar results (discrepancy less than 3%), however we believe that the image analysis is more accurate. Hence, we adopted this method for all samples, except for UM1_E4 sample which was broken in several irregular shaped chips (brittle failure) and the archimedean buoyancy was used (Fig. 5a).

The bulk volume incorporates the volume of the rock (V_{DRE}), as well as, the volume of connected ($V_{\phi C}$) and isolated ($V_{\phi I}$) porosity.

$$\rho_B = \frac{M_R}{\left(V_{DRE} + V_{\phi_C} + V_{\phi_I}\right)} \quad \text{(A.6)}$$

The values of bulk density (ρ_B), skeletal density (ρ_{sk}) and dense rock equivalent density (ρ_{DRE}) of the samples were finally used to extract the values of connected (ϕ_C), total (ϕ_T) and isolated (ϕ_I) according to the following relationships:

$$\phi_C = 1 - \frac{\rho_B}{\rho_{sk}} \quad \text{(A.7)}$$

$$\phi_T = 1 - \frac{\rho_B}{\rho_{DRE}} \quad \text{(A.8)}$$

$$\phi_I = \frac{\rho_B}{\rho_{sk}} - \frac{\rho_B}{\rho_{DRE}} \quad \text{(A.9)}$$

Appendix B. The Volcanology Deformation Rig (VDR)

The unit performs both constant displacement rate and constant load tests. Displacement is achieved by controlling the position of the bottom platen using an electronic stepper motor with a displacement speed range from 5×10^{-6} to 2.5×10^{-2} cm/s and measured using a built-in linear variable differential transformer (LVDT) displacement transducer with a 7.6 cm travel range and 0.00013 cm resolution. Load is measured using an S-type load cell attached to a fixed crossarm.

Samples can be loaded at rates from zero to 1.9 kg/s, and the maximum attainable load is 1136 kg with 0.086 kg resolution. High temperatures are attained by a Zircar-type FIH fiber insulated heater tube furnace. The furnace has helically wound, Fe-Cr-Al alloy resistance wire elements embedded in a rigid body of high-temperature refractory fiber. It is 30.5 cm long, and has inner and outer diameters of 7.6 and 15.25 cm, respectively. It is seated on the steel base and surrounds the lower piston, the sample and most of the upper piston. The furnace generates

temperatures up to 1100 °C. A K-type thermocouple is used to monitor and control temperature during the experiment.

The press was calibrated on solid glass cores (10 × 25 mm) of NIST (NBS) standard reference material (SRM) 717a (borosilicate glass) under constant load and dry conditions at temperatures (550–600 °C; see Robert et al., 2008a). The resulting experimental accuracy corresponds to 0.2 log units (Robert et al. 2008a).

References

Ardia, P., Giordano, D., Schmidt, M.W., 2008. A model for the viscosity of rhyolite as a function of H2O-content pressure: A calibration based on centrifuge piston cylinder experiments. Geochimica Et Cosmochimica Acta 72, 6103-6123. doi: 10.1016/j.gca.2008.08.025.

Avard, G., Whittington, A.G., 2012. Rheology of arc dacite lavas: experimental determination at low strain rates. Bulletin of Volcanology 1039–1056, doi: 10.1007/s00445-012-0584-2.

Bagdassarov, N.S., Dingwell, D.B., 1992. A rheological investigation of vesicular rhyolite. Journal of Volcanology and Geothermal Research 50, 307-322.

Bagdassarov, N.S., Dingwell, D.B., 1993. Deformation of foamed rhyolites under internal and external stresses: an experimental investigation. Bulletin of Volcanology 55, 147-154.

Bruckner, R., Deubener, J., 1997. Description and interpretation of the two phase flow behaviour of melts with suspended crystals. Journal of Non-Crystalline Solids 209, 283-291.

Caricchi, L., Burlini, L., Ulmer, P., Gerya, T., Vassalli, M., Papale, P., 2007. Non-Newtonian rheology of crystal-bearing magmas and implications for magma ascent dynamics. Earth and Planetary Science Letters 264, 402-419. doi: 10.1016/j.epsl.2007.09.032.

Caricchi, L., Giordano, D., Burlini, L., Ulmer, P., Romano, C., 2008. Rheological properties of magma from the 1538 eruption of Monte Nuovo (Phlegrean Fields, Italy): An experimental study. Chemical Geology 256, 158-171. doi: 10.1016/j.chemgeo.2008.06.035.

Cimarelli, C., Costa, A., Mueller, S., Mader, H.M., 2011. Rheology of magmas with bimodal crystal size and shape distributions: Insights from analog experiments. Geochemistry Geophysics Geosystems 12, 1-14. doi: 10.1029/2011GC003606.

Cordonnier, B., Hess, K.-U., Lavallée, Y., and Dingwell, D.B., 2009. Rheological properties of dome lavas: Case study of Unzen volcano. Earth and Planetary Science Letters 279, 263–272, doi: 10.1016/j.epsl.2009.01.014.

Costa, A., 2005. Viscosity of high crystal content melts: dependence on solid fraction. Geophysical Research Letters 32, 5 pp. doi: 10.1029/2005gl024303.

Costa, A., Caricchi, L., Bagdassarov, N.S., 2009. A model for the rheology of particle-bearing suspensions and partially molten rocks. Geochemistry Geophysics Geosystems 10, 1-13. doi: 10.1029/2008gc002138.

Deubener, J., Bruckner, R., 1997. Influence of nucleation and crystallisation on the rheological properties of lithium disilicate melt. Journal of Non-Crystalline Solids 209, 96-111.

Di Vito, M.A., Lirer, L., Mastrolorenzo, G., Rolandi, G., 1987. The Monte Nuovo eruption (Campi Flegrei, Italy). Bulletin of Volcanology 49, 608–615.

Dingwell, D.B., 2006. Transport Properties of Magmas: Diffusion and Rheology. Elements 2, 281-286. doi: 10.2113/gselements.2.5.281.

Dingwell, D.B., Virgo, D., 1987. The effect of oxidation state on the viscosity of melts in the system Na2O-FeO-Fe2O3-SiO2. Geochimica et Cosmochimica Acta 51, 195-205.

Dingwell, D.B., Webb, S.L., 1990. Relaxation in silicate melts. European Journal of Mineralogy 2, 427-449.

Dingwell, D.B., Romano, C., Hess, K.U., 1996. The effect of water on the viscosity of a haplogranitic melt under P-T-X conditions relevant to silicic volcanism. Contributions to Mineralogy and Petrology 124, 19-28.

D'Oriano, C., Poggianti, E., Bertagnini, A., Cioni, R., Landi, P., Polacci, M., Rosi, M., 2005. Changes in eruptive style during the A.D. 1538 Monte Nuovo eruption (Phlegrean Fields, Italy): the role of syn-eruptive crystallization. Bulletin of Volcanology 67, 601-621. doi: 10.1007/s00445-004-0397-z.

Einstein, A., 1906. Eine neue Bestimmung der Molekul-dimensionen. Ann. Phys. 19, 289-306.

Frankel, N.A., Acrivos, A., 1967. On the viscosity of a concentrated suspension of solid spheres. Chemical Engineering Science 22, 847-853.

Gay, E.C., Nelson, P.A., Armstrong, W.P., 1969. Flow properties of suspensions with high solids concentration. Aiche Journal 15, 815-822.

Giordano, D., Dingwell, D.B., 2003. Non-Arrhenian multicomponent melt viscosity: a model. Earth and Planetary Science Letters 208, 337-349. doi: 10.1016/s0012-821x(03)00042-6.

Giordano, D., Romano, C., Papale, P., Dingwell, D.B., 2004. The viscosity of trachytes, and comparison with basalts, phonolites, and rhyolites. Chemical Geology 213, 49-61. doi: 10.1016/j.chemgeo.2004.08.032.

Giordano, D., Nichols, A.R.L., Dingwell, D.B., 2005. Glass transition temperatures of natural hydrous melts: a relationship with shear viscosity and implications for the welding process. Journal of Volcanology and Geothermal Research 142, 105-118. doi: 10.1016/j.jvolgeores.2004.10.015.

Giordano, D., Mangiacapra, A., Potuzak, M., Russell, J.K., Romano, C., Dingwell, D.B., Di Muro, A., 2006. An expanded non-Arrhenian model for silicate melt viscosity: A treatment for metaluminous, peraluminous and peralkaline liquids. Chemical Geology 229, 42-56. doi: 10.1016/j.chemgeo.2006.01.007.

Giordano, D., Russell, J.K., Dingwell, D.B., 2008. Viscosity of magmatic liquids: A model. Earth and Planetary Science Letters 271, 123-134. doi: 10.1016/j.epsl.2008.03.038.

Giordano, D., Ardia, P., Romano, C., Dingwell, D.B., Di Muro, A., Schmidt, M.W., Mangiacapra, A., Hess, K.U., 2009. The rheological evolution of alkaline Vesuvius magmas and comparison with alkaline series from the Phlegrean Fields, Etna, Stromboli and Teide. Geochimica et Cosmochimica Acta 73, 6613-6630. doi: 10.1016/j.gca.2009.07.033.

Gonnermann, H.M., Manga, M., 2005. Flow banding in obsidian: A record of evolving textural heterogeneity during magma deformation. Earth and Planetary Science Letters 236, 135-147. doi: 10.1016/j.epsl.2005.04.031.

Harris, A.J.L., Allen III, J.S., 2008. One-, two- and three-phase viscosity treatments for basaltic lava flows. Journal of geophysical research 113, B09212, doi: 10.1029/2007JB005035.

Hess, K.-U., Cordonnier, B., Lavallée, Y., Dingwell, D.B., 2007. High-load, high-temperature deformation apparatus for synthetic and natural silicate melts. The Review of scientific instruments 78, 7, 075102, doi: 10.1063/1.2751398.

Herschel, W.H., Bulkley, R., 1926. Konsistenzmessungen von Gummi-Benzollösungen. KolloidZeitschrift 39, 291-300. doi: 10.1007/BF01432034.

Hinch, E.J., Acrivos, A., 1980. Long slender drops in a simple shear flow. Journal of Fluid Mechanics 98, 305-328. doi: 10.1017/S0022112080000171.

Hui, H.J., Zhang, Y., 2007. Toward a general viscosity equation for natural anhydrous and hydrous silicate melts. Geochimica Et Cosmochimica Acta 71, 403-416. doi: 10.1016/j.gca.2006.09.003.

Ishibashi, H., 2009. Non-Newtonian behavior of plagioclase-bearing basaltic magma: Subliquidus viscosity measurement of the 1707 basalt of Fuji volcano, Japan. Journal of Volcanology and Geothermal Research 181, 78-88. doi: 10.1016/j.jvolgeores.2009.01.004.

Ishibashi, H., Sato, H., 2007. Viscosity measurements of subliquidus magmas: Alkali olivine basalt from the Higashi-Matsuura district, Southwest Japan. Journal of Volcanology and Geothermal Research 160, 223-238. doi: 10.1016/j.jvolgeores.2006.10.001.

Kohlstedt, D.L., Zimmerman, M.E., 1996. Rheology of partially molten mantle rocks. Annual Review of Earth and Planetary Sciences 24, 41-62.

Kohlstedt, D.L., Holtzman, B.K., 2009. Shearing Melt Out of the Earth: An Experimentalist's Perspective on the Influence of Deformation on Melt Extraction. Annual Review of Earth and Planetary Sciences 37, 561-593. doi: 10.1146/annurev.earth.031208.100104.

Krieger, I.M., 1972. Rheology of monodisperse latices. Advances in Colloid and Interface Science 3, 111-136.

Krieger, I.M., Dougherty, T.J., 1959. A Mechanism for Non-Newtonian Flow in Suspensions of Rigid Spheres. Journal of Rheology 3, 137-152.

Lavallée, Y., Hess, K.-U., Cordonnier, B., Dingwell, D.B., 2007. Non-Newtonian rheological law for highly crystalline dome lavas. Geology 35, 843. doi: 10.1130/G23594A.1.

Lavallée, Y., Meredith, P.G., Dingwell, D.B., Hess, K.-U., Wassermann, J., Cordonnier, B., Gerik, A., Kruhl, J.H., 2008. Seismogenic lavas and explosive eruption forecasting. Nature 453, 507–510, doi: 10.1038/nature06980.

Lavallée, Y., Mitchell, T.M., Heap, M.J., Vasseur, J., Hess, K.-U., Hirose, T., Dingwell, D.B., 2012. Experimental generation of volcanic pseudotachylytes: Constraining rheology. Journal of Structural Geology 38, doi: 10.1016/j.jsg.2012.02.001.

Lejeune, A.M., Richet, P., 1995. Rheology of crystal-bearing silicate melts - An experimental study at high viscosities. Journal of Geophysical Research-Solid Earth 100, 4215-4229.

Lejeune, A.M., Bottinga, Y., Trull, T.W., Richet, P., 1999. Rheology of bubble-bearing magmas. Earth and Planetary Science Letters 166, 71-84.

Llewellin, E.W., Manga, M., 2005. Bubble suspension rheology and implications for conduit flow. Journal of Volcanology and Geothermal Research 143, 205-217. doi: 10.1016/j.jvolgeores.2004.09.018.

Llewellin, E.W., Mader, H.M., Wilson, S.D.R., 2002. The rheology of a bubbly liquid. Proceedings of the Royal Society of London Series a-Mathematical Physical and Engineering Sciences 458, 987-1016. doi: 10.1098/rspa.2001.0924.

Manga, M., Loewenberg, M., 2001. Viscosity of magmas containing highly deformable bubbles. Journal of Volcanology and Geothermal Research 105, 19-24.

Manga, M., Castro, J.M., Cashman, K.V., Loewenberg, M., 1998. Rheology of bubble-bearing magmas. Journal of Volcanology and Geothermal Research 87, 15-28.

Maron, S.H., Pierce, P.E., 1956. Application of ree-eyring generalized flow theory to suspensions of spherical particles. Journal of Colloid Science 11, 80-95.

Maxwell, J.C., 1867. On the Dynamical Theory of Gases. Philosophical Transactions of the Royal Society of London 157, 49-88.

McBirney, A.R., Murase, T., 1984. Rheological Properties of Magmas. Annual Review of Earth and Planetary Sciences 12, 337-357. doi:10.1146/annurev.ea.12.050184.002005.

Misiti, V., Vetere, F., Mangiacapra, A., Behrens, H., Cavallo, A., Scarlato, P., Dingwell, D.B., 2009. Viscosity of high-K basalt from the 5th April 2003 Stromboli paroxysmal explosion. Chemical Geology 260, 278-285. doi: 10.1016/j.chemgeo.2008.12.023.

Mogi, K., 1966. Some precise measurements of fracture strength of rock under uniform compressive stress.. Rock Mechanics and Engineering Geology 4, 41–55.

Mueller, S., Llewellin, E.W., Mader, H.M., 2010. The rheology of suspensions of solid particles. Proceedings of the Royal Society a-Mathematical Physical and Engineering Sciences 466, 1201-1228. doi: 10.1098/rspa.2009.0445.

Mungall, J.E., Bagdassarov, N.S., Romano, C., Dingwell, D.B., 1996. Numerical modelling of stress generation and microfracturing of vesicle walls in glassy rocks. Journal of Volcanology and Geothermal Research 73, 33-46.

Pal, R., 2003. Rheological behavior of bubble-bearing magmas. Earth and Planetary Science Letters 207, 165-179. doi: 10.1016/S0012-821X(02)01104-4.

Papale, P., 1999. Strain-induced magma fragmentation in explosive eruptions. Nature 397, 425-428.

Petford, N., 2009. Which effective viscosity?. Mineralogical Magazine 73, 167-191. doi: 10.1180/minmag.2009.073.2.167.

Phan-Thien, N., and Pham, D.C., 1997. Differential multiphase models for polydispersed suspensions and particulate solids. Journal of Non-Newtonian Fluid Mechanics, 72, 305–318.

Picard, D., Arbaret, L., Pichavant, M., Champallier, R., Launeau, P., 2011. Rheology and microstructure of experimentally deformed plagioclase suspensions. Geology 39, 8, 747–750, doi: 10.1130/G2217.1.

Pinkerton, H., Stevenson, R.J., 1992. Methods of determining the rheological properties of magmas at sub-liquidus temperatures. Journal of Volcanology and Geothermal Research 53, 47-66.

Pinkerton, H., Norton, G.E., 1995. Rheological properties of basaltic lavas at sub-liquidus temperatures: laboratory field measurements on lavas from Mount Etna. Journal of Volcanology and Geothermal Research 68, 307-323.

Piochi, M., Mastrolorenzo, G., Pappalardo, L., 2005. Magma ascent and eruptive processes from textural and compositional features of Monte Nuovo pyroclastic products, Campi Flegrei, Italy. Bulletin of Volcanology 67, 663-678. doi: 10.1007/s00445-005-0410-1.

Piochi, M., Polacci, M., De Astis, G., Zanetti, A., Mangiacapra, A., Vannucci, R., Giordano, D., 2008. Texture and composition of pumices and scoriae from the Campi Flegrei caldera (Italy): Implications on the dynamics of explosive eruptions. Geochemistry Geophysics Geosystems 9, Q03013. doi: 10.1029/2007gc001746.

Quane, S.L., Russell, J.K., 2005. Welding: insights from high-temperature analogue experiments. Journal of Volcanology and Geothermal Research 142, 67-87. doi: 10.1016/j.jvolgeores.2004.10.014.

Quane, S.L., Russell, J.K., 2006. Bulk and particle strain analysis in high-temperature deformation experiments. Journal of Volcanology and Geothermal Research 154, 63-73. doi: 10.1016/j.jvolgeores.2005.09.025.

Quane, S.L., Russell, J.K., Kennedy, L.A., 2004. A low-load, high-temperature deformation apparatus for volcanological studies. American Mineralogist 89, 873-877.

Richet, P., Lejeune, A.M., Holtz, F., Roux, J., 1996. Water and the viscosity of andesite melts. Chemical Geology 128, 185-197.

Robert, G., Russell, J.K., Giordano, D., Romano, C., 2008a. High-temperature deformation of volcanic materials in the presence of water. American Mineralogist 93, 74-80. doi: 10.2138/am.2008.2665.

Robert, G., Russell, J.K., Giordano, D., 2008b. Rheology of porous volcanic materials: High-temperature experimentation under controlled water pressure. Chemical Geology 256, 216-230. doi: 10.1016/j.chemgeo.2008.06.028.

Romano, C., Mungall, J.E., Sharp, T.G., Dingwell, D.B., 1996. Tensile strengths of hydrous vesicular glasses: An experimental study. American Mineralogist 81, 1148-1154.

Romano, C., Poe, B.T., Mincione, V., Hess, K.U., Dingwell, D.B., 2001. The viscosities of dry and hydrous XAlSi3O8 (X = Li, Na, K, Ca-0.5, Mg-0.5) melts. Chemical Geology 174, 115-132.

Romano, C., Giordano, D., Papale, P., Mincione, V., Dingwell, D.B., Rosi, M., 2003. The dry and hydrous viscosities of alkaline melts from Vesuvius and Phlegrean Fields. Chemical Geology 202, 23-38. doi: 10.1016/s0009-2541(03)00208-0.

Russell, J.K., Giordano, D., Dingwell, D.B., Hess, K.U., 2002. Modelling the non-Arrhenian rheology of silicate melts: Numerical considerations. European Journal of Mineralogy 14, 417-427. doi: 10.1127/0935-1221/2002/0014-0417.

Russell, J.K., Giordano, D., Dingwell, D.B., 2003. High-temperature limits on viscosity of non-Arrhenian silicate melts. American Mineralogist 88, 1390-1394.

Rust, A.C., Manga, M., 2002. Effects of bubble deformation on the viscosity of dilute suspensions. Journal of Non-Newtonian Fluid Mechanics 104, 53-63.

Rybacki, E., Dresen, G., 2004. Deformation mechanism maps for feldspar rocks. Tectonophysics 382, 173-187. doi: 10.1016/j.tecto.2004.01.006.

Ryerson, F.J., Weed, H.C., Piwinskii, A.J., 1988. Rheology of subliquidus magmas 1. Picritic compositions. Journal of Geophysical Research-Solid Earth and Planets 93, 3421-3436.

Sato, H., 2005. Viscosity measurement of subliquidus magmas: 1707 basalt of Fuji volcano. Journal of Mineralogical and Petrological Sciences 100, 133-142.

Shaw, H.R., 1965. Comments on viscosity, crystal settling, and convection in granitic magmas. Am. J. Sci. 263, 120-152.

Shaw, H.R., 1969. Rheology of Basalt in the Melting Range. J. Petrology 10, 510-535. doi: 10.1093/petrology/10.3.510.

Sparks, R.S.J., Pinkerton, H., 1978. Effects of degassing on rheology of basaltic lava. Nature 276, 385-386.

Spera, F.J., Borgia, A., Strimple, J., Feigenson, M., 1988. Rheology of melts and magmatic suspensions 1. Design and calibration of concentric cylinder viscometer with application to rhyolitic magma. Journal of Geophysical Research-Solid Earth and Planets 93, 10273-10294.

Stein, D.J., Spera, F.J., 1992. Rheology And Microstructure Of Magmatic Emulsions - Theory And Experiments. Journal of Volcanology and Geothermal Research 49, 157-174.

Stein, D.J., Spera, F.J., 2002. Shear viscosity of rhyolite-vapor emulsions at magmatic temperatures by concentric cylinder rheometry. Journal of Volcanology and Geothermal Research 113, 243-258.

Stevenson, R.J., Bagdassarov, N.S., Dingwell, D.B., Romano, C., 1998. The influence of trace amounts of water on the viscosity of rhyolites. Bulletin of Volcanology 60, 89-97.

Stickel, J.J., Powell, R.L., 2005. Fluid mechanics and rheology of dense suspensions. Annual Review of Fluid Mechanics 37, 129-149. doi: 10.1146/annurev.fluid.36.050802.122132.

Taylor, G.I., 1932. The Viscosity of a Fluid Containing Small Drops of Another Fluid. Proceedings of the Royal Society of London Series A Containing Papers of a Mathematical and Physical Character 19051934 138, 41-48. doi: 10.1098/rspa.1932.0169.

Tuffen, H., Dingwell, D.B., Pinkerton, H., 2003. Repeated fracture and healing of silicic magma generate flow banding and earthquakes?. Geology 31, 1089-1092. doi: 10.1130/G19777.1.

Vetere, F., Behrens, H., Misiti, V., Ventura, G., Holtz, F., De Rosa, R., Deubener, J., 2007. The viscosity of shoshonitic melts (Vulcanello Peninsula, Aeolian Islands, Italy): Insight on the magma ascent in dikes. Chemical Geology 245, 89-102. doi: 10.1016/j.chemgeo.2007.08.002.

Vetere, F., Behrens, H., Schuessler, J.A., Holtz, F., Misiti, V., Borchers, L., 2008. Viscosity of andesite melts and its implication for magma mixing prior to Unzen 1991-1995 eruption. Journal of Volcanology and Geothermal Research 175, 208-217. doi: 10.1016/j.jvolgeores.2008.03.028.

Vona, A., Romano, C., Dingwell, D.B., Giordano, D., 2011. The rheology of crystal-bearing basaltic magmas from Stromboli and Etna. Geochimica et Cosmochimica Acta 75, 3214-3236. doi: 10.1016/j.gca.2011.03.031.

Webb, S.L., Dingwell, D.B., 1990a. Non-Newtonian Rheology of Igneous Melts at High Stresses and Strain Rates: Experimental Results for Rholite, Andesite, Basalt, and Nephelinite. Journal of Geophysical Research-Solid Earth and Planets 95, 15695-15701.

Webb, S.L., Dingwell, D.B., 1990b. The Onset of Non-Newtonian Rheology of Silicate Melts. Physics and Chemistry of Minerals 17, 125-132.

Whittington, A., Richet, P., Holtz, F., 2000. Water and the viscosity of depolymerized aluminosilicate melts. Geochimica Et Cosmochimica Acta 64, 3725-3736.

Whittington, A., Richet, P., Linard, Y., Holtz, F., 2001. The viscosity of hydrous phonolites and trachytes. Chemical Geology 174, 209-223.

Whittington, A.G., Hellwig, B., Behrens, H., Joachim, B., Stechern, A., Vetere, F., 2009. The viscosity of hydrous dacitic liquids: implications for the rheology of evolving silicic magmas. Bulletin of Volcanology 71 185–199, doi: 10.1007/s00445-008-0217-y.

Whittington, A.G., Richet, P., Polian, A., 2012. Water and the compressibility of silicate glasses: A Brillouin spectroscopic study. American Mineralogist 97, 2-3, 455–467, doi: 10.2138/am.2012.3891.

Figure Captions

Fig. 1. Density and porosity characterization of the analyzed specimen from Monte Nuovo. (a) Bulk density (ρ_B) vs. connected porosity (ϕ_C). Connected porosity was calculated taking the difference between the core volume and the volume measured by pycnometry. Bulk density is the ratio between the sample weight and the volume of the core. Grey circles: LM samples; empty squares: UM (UM1+UM2) samples. Filled squares represent the UM1 samples used for deformation experiments. Star symbol represents the value of dense rock equivalent (DRE) density measured by pycnometry on both LM and UM sample powders. (b) Total porosity distributions for LM and UM cores.

Fig. 2. (a) Characteristic relaxation timescale (τ) – temperature relationship for Monte Nuovo anhydrous trachytic liquid determined using the Maxwell relationship (Dingwell and Webb, 1990) Monte Nuovo liquid viscosity refers to the fitting of measured data by Giordano et al. (2004; 2009) Vertical dashed lines represent experimental temperatures from this study. Gray horizontal bars shows characteristic relaxation timescales used to define minimum experimental dwell times. (b)

Characteristic relaxation timescale (τ) – characteristic relaxation rate ($\dot{\varepsilon}_{relax} = \tau^{-1}$) - temperature relationship for Monte Nuovo anhydrous trachytic liquids. Brittle failure (dark grey) and Non-Newtonian behavior (light grey) fields are calculated according to Dingwell and Webb (1990) as 2 and 3 $\log_{10}$ units above the relaxation curve, respectively. The vertical dashed lines represent experimental temperatures from this study. Horizontal dashed lines are iso-strain-rate curves at $\dot{\varepsilon}_{relax}$ = 10^{-4}, 10^{-5}, 10^{-6}, 10^{-7} s^{-1}. Black dots indicate the strain rate and temperature conditions of the deformation experiments.

Fig. 3. Results of constant displacement rate experiments. (a) Stress (due to the applied load) plotted against instrumental strain (ε_m) for experiments involving different constant displacement-rates (idenitified as I - VII for UM1_E10 and I-III for UM1_B14) and run at T=750°C (UM1_E10: black line and segments I-VII; and UM1_B14: gray line and segments I-III). The corresponding strain rates for UM1_E10 are: (I) $\dot{\varepsilon}$ =1.0 x 10^{-5} s^{-1}; (II) $\dot{\varepsilon}$ =1.0 x 10^{-6} s^{-1}; (III) $\dot{\varepsilon}$ =5.3 x 10^{-5} s^{-1}; (IV) $\dot{\varepsilon}$ =1.1 x 10^{-5} s^{-1}; (V) $\dot{\varepsilon}$ =1.1 x 10^{-6} s^{-1}; (VI) $\dot{\varepsilon}$ =1.2 x 10^{-7} s^{-1}; (VII) $\dot{\varepsilon}$ =3.3 x 10^{-6} s^{-1}. For UM1_B14 sample, strain rates are: (I) $\dot{\varepsilon}$ =2.9 x 10^{-5} s^{-1}; (II) $\dot{\varepsilon}$ =5.6 x 10^{-5} s^{-1}; (III) $\dot{\varepsilon}$ =9.6 x 10^{-5} s^{-1}. (b) First deformation segment for sample UM1_E10 (I) conducted at T=750°C and at a constant displacement rate translating to strain rate of 1.0 x 10^{-5} s^{-1} (Strain vs. Time curve slope in the inset). Apparent viscosity is calculated as $\sigma/\dot{\varepsilon}$.

Fig. 4. Evolution of applied stress and apparent viscosity with increasing strain and time at (a) T=600°C (UM1_E4 (I)) and (b) T=800°C (UM1_A12 (IV)). In (b), strain axis starts from ε = 0.04, as previous deformation steps for this sample amounted to ε = 0.04.

Fig. 5. (a) Post-run characterization of experimental cores. Photograph of sample core (UM1_E4) and scanned image of thin sections (UM1_E1B; UM1_B14; UM1_A12) at the end of high temperature deformation experiments. Dashed rectangles represent pre-run core geometry; arrows indicate direction of load: The total strain (ε) undergone by samples is also reported. (b-c) Optical photomicrographs of UM1 sample (b) before deformation and (b) at the end of deformation experiment at T=800°C (UM1_A12).

Fig. 6. (a) Connected (ϕ_c; circles) and isolated (ϕ_i; triangles) porosity distribution in pre- and post-run sample cores (empty and filled symbols, respectively) as a function of total porosity (ϕ_T). Gray shaded areas define the distribution of all the analyzed material (see Fig. 1). (b-c) Partitioning of strain analysis according to Quane and Russell (2006): (b) manually measured strain (ε_s) compared to the sum of axial (ε_a) and radial (ε_r) strain. (c) Comparison of axial (ε_a) and radial (ε_r) strain components. Dashed lines are iso-strain. With increasing total strain, radial component becomes dominant (grey arrow).

Fig. 7. (a) Stress vs. strain rate plot for UM1 samples at different temperatures and (b) variation of apparent viscosity as a function of applied strain rate. Horizontal error bars denote uncertainties on shear rate determination due to instrumental displacement resolution and core length determination; if not reported, error bars are smaller than symbols. Black lines represent the fitting results using Eq. (24). Grey horizontal lines in (b) indicate pure liquid viscosity after Giordano et al. (2009) at experimental temperatures.

Fig. 8. Summary of relationships between flow parameters and temperature. (a) Consistency *K* – temperature and (b) flow index *n* – temperature plots. Symbols denote values obtained from Eq. (24). Linear regression (solid line) parameters are reported in Table 5. (c) Measured viscosity

compared to viscosity calculated with Eqs. (25-28). Solid line represent 1:1 relationship, dashed lines indicate ± 0.25 and ± 0.50 $\log_{10}$ units discrepancies.

Fig. 9. Combined effect of pores and crystals on the rheology of Monte Nuovo magmas as a function of (a) temperature and (b) crystal fraction. Relative viscosity (η_r) is calculated by normalizing the measured values of apparent viscosity to the viscosity of the pure liquid after Giordano et al. (2009) (dashed line). (a) Logarithm of relative viscosity vs. temperature at different strain rates ($\dot{\varepsilon}$). (b) Relative viscosity as a function of sample crystal fraction (ϕ_{xls}). Two (liquid + crystals; black lines) and three phases (liquid + crystals + bubbles; blue lines) parameterizations are also shown for comparison. Two phases parameterization is calculated after Vona et al. (2011) (Eq. 10) at $\dot{\varepsilon} = 10^{-6}$, 10^{-5} and 10^{-4} s^{-1}. Three phases mixture viscosities are calculated after Phan-Thien and Pham (1997) (Eqs. 19-21).

Tables

Table 1

Pre- and post-run characterization of investigated materials.

		Pre-run							Post-run										
	(°C)	i	i	B	sk	T	C	I	f	f	B	sk	T	C	I	m	s	a	r
M1_E4	00	2.89	2.85	.563	.576	.406	.393	.012			*.56*	*.58*	*.40*	*.39*	*.01*				
												6	*6*	*6*	*0*				
M1_E7	40	9.99	2.83	.423	.587	.459	.450	.009	8.12	2.95	.452	.589	.448	.439	.009	.057	.047	.021	.018
M1_E1B	00	0.66	2.84	.542	.549	.414	.395	.018	9.22	2.97	.563	.562	.405	.390	.016	.037	.035	.014	.019
M1_E2A	25	0.37	2.83	.524	.595	.420	.413	.008	8.47	3.03	.537	.604	.415	.410	.006	.067	.047	.008	.030
M1_E10	50	7.78	0.97	.359	.563	.483	.470	.013	9.31	1.66	.446	.574	.450	.438	.012	.177	.177	.060	.113
M1_B14	50	0.05	0.97	.477	.589	.438	.429	.009	5.61	1.23	.547	.593	.412	.403	.008	.122	.111	.045	.046
M1_E1A	00	7.39	2.85	.499	.549	.430	.412	.018	6.20	2.95	.529	.554	.419	.402	.017	.046	.046	.019	.015

M1_	00	0.0	0.9	.52	.61	.42	.41	.00	*1.3*	*3.9*	*.75*	*.61*	*.33*	*.32*	*.00*	*.45*	*.46*	*.13*	*.38*
A12		4	7	1	0	2	7	4	*8*	*8*	*3*	*1*	*3*	*8*	*5*	*5*	*6*	*3*	*4*

Pre- and post – run core geometry (length L and radius r) is expressed in mm. Densities (ρ_B and ρ_{sk}) are expressed in g/cm^3. Strain parameters are: instrumental strain (ε_m), sample strain (ε_s), axial strain (ε_a) and radial strain (ε_r). Values in italics print represent measurements with high uncertainities.

Table. 2

Electron microprobe analyses (wt% oxides) of UM samples.

	Bulk Rock[a]	Matrix Glass[a]
SiO_2	60.33	61.66
TiO_2	0.43	0.57
Al_2O_3	19.39	19.48
FeO	3.23	3.55
MgO	0.24	0.34
MnO	0.22	0.25
CaO	1.79	1.11
Na_2O	5.85	4.85
K_2O	7.21	7.85
P_2O_5	0.02	0.04
Total	98.70	99.69

[a]Chemical analyses from Caricchi et al. (2008)

Table 3 Summary of the performed experiments

Sample	(°C)	Initial Porosity (ϕ_T)	Deformation Step	Strain Rate (s^{-1})	Stress (MPa)	Instrumental Strain (ε_m)	log η_{matrix}	log η_{app}	log η_r
M1_E4	U 00	0.41	I	*.6E-06*	*5.25*	-	*3.59*	*2.42*	
M1_E7	U 40	0.46	I	.8E-06	.52	0.022	2.74	2.48	0.26
			II	.0E-06	.64	0.009	2.74	2.51	0.23
			III	.6E-06	2.32	0.027	2.74	2.34	0.40
M1_E1B	U 00	0.41	I	.1E-06	.08	0.015	1.20	2.12	.92
			II	.1E-06	.73	0.014	1.20	1.89	.69
			III	.0E-06	.42	0.007	1.20	2.38	.19
			IV	.1E-07	.55	0.001	1.20	3.15	
M1_E2A	U 25	0.42	I	.8E-06	.69	0.028	0.62	1.44	.81
			II	.8E-06	.14	0.007	0.62	1.57	.94
			III	.8E-06	.68	0.007	0.62	1.78	.15
			IV	.8E-07	.29	0.005	0.62	2.12	.50
			V	.9E-05	.78	0.021	0.62	1.30	.68
M1_E10	U 50	0.48	I	.0E-05	.00	0.030	0.10	1.00	.90
			II	.0E-06	.50	0.006	0.10	1.70	.60
			III	.3E-05	.89	0.037	0.10	0.74	.64
			IV	.1E-05	.16	0.048	0.10	1.02	.92
			V	.1E-06	.49	0.005	0.10	1.65	.55
			VI	.2E-07	.34	0.001	0.10	2.45	
			VII	.3E-06	.33	0.063	0.10	1.61	.50
M1_B14	U 50	0.44	I	.9E-05	.44	0.038	0.10	0.92	.82
			II	.6E-05	.24	0.033	0.10	0.76	.66
			III	.6E-05	.16	0.056	0.10	0.64	.54
M1_E1A	U 00	0.43	I	.9E-06	.00	0.025	.15	1.54	.39
			II	.7E-06	.53	0.023	.15	1.43	.28
M1_A12	U 00	0.42	I	.1E-05	.79	0.016	.15	1.21	.06
			II	.1E-05	.23	0.011	.15	0.86	.71
			III	.8E-05	.59	0.014	.15	0.65	.50

IV	*.0E-04*	*.86*	*0.432*	.15	*0.46*

Values in italic print represent measurements at which a constant stress at flow was not achieved due to the failure of the sample (UM1_E4) or the onset of shear weakening (UM1_A12). In this case, peak stress is reported.

Table 4

Fitting parameters of experimental data

	Herschel- Bulkely fit							*Power Law fit*				
	σ_o		log K		n		^{2}	log K		n		^{2}
(°C)	MPa)	.e. (%)	Pa s)	.e. (%)		.e. (%)		Pa s)	.e. (%)		.e. (%)	
40	.40e-9	100	.56	100	.470	100	.955	.60	.76	.48	4.97	.941
00	.74e-9	100	.53	100	.353	100	.964	.67	.15	.38	6.95	.972
25	.988	5.04	.94	3.05	.741	.63	.999	.23	.15	.36	.30	.975
50	.161	100	.00	9.45	.595	6.63	.986	.49	.98	.47	.17	.970
00	.00e-10	100	.55	100	.267	100	.962	.67	.77	.29	4.74	.939

Table 5

Flow parameter (log K and n) vs. temperature fitting results

log K					
c_k	s.e. (%)[a]	m_k	s.e. (%)[a]	r^2	
6.722	1.84	8	0.0113	-7.70	1.911
n					
c_n	s.e. (%)[a]	m_n	s.e. (%)[a]	r^2	
.0255	1.52	1	0.0009	-6.53	1.964

c and m represent intercept and slope of the linear regressions.

[a] standard error expressed as percentage of fitting parameter.

Highlights

We performed experiments to estimate the rheological evolution of Monte Nuovo magmas

We examine how crystals and bubbles influences the rheological behavior of magmas

The presence of pore may produce a marked decrease of their viscosity.

The presence of pores leads to a strong decrease in the strength of magmas

Figure 1

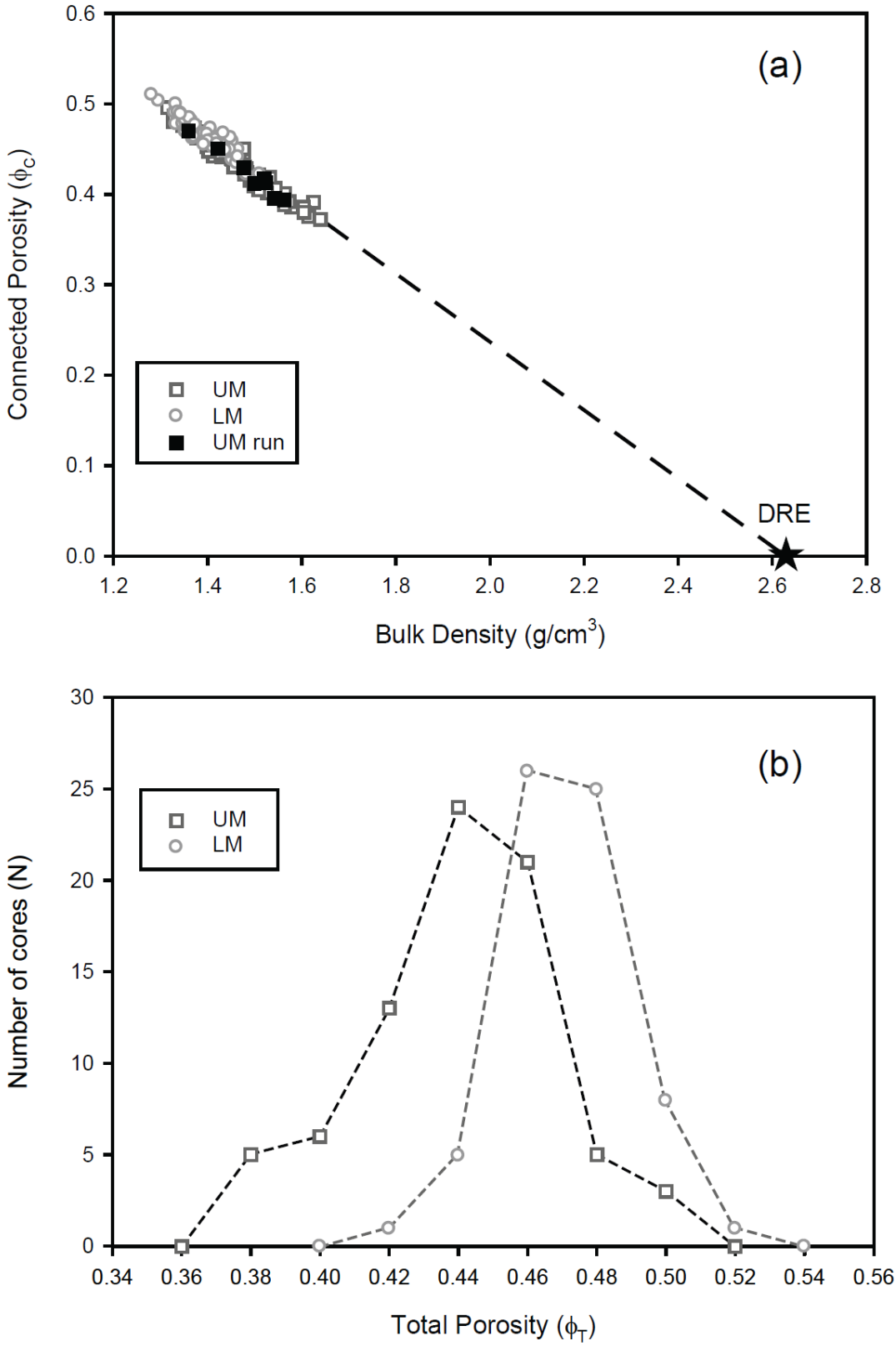

Figure 2

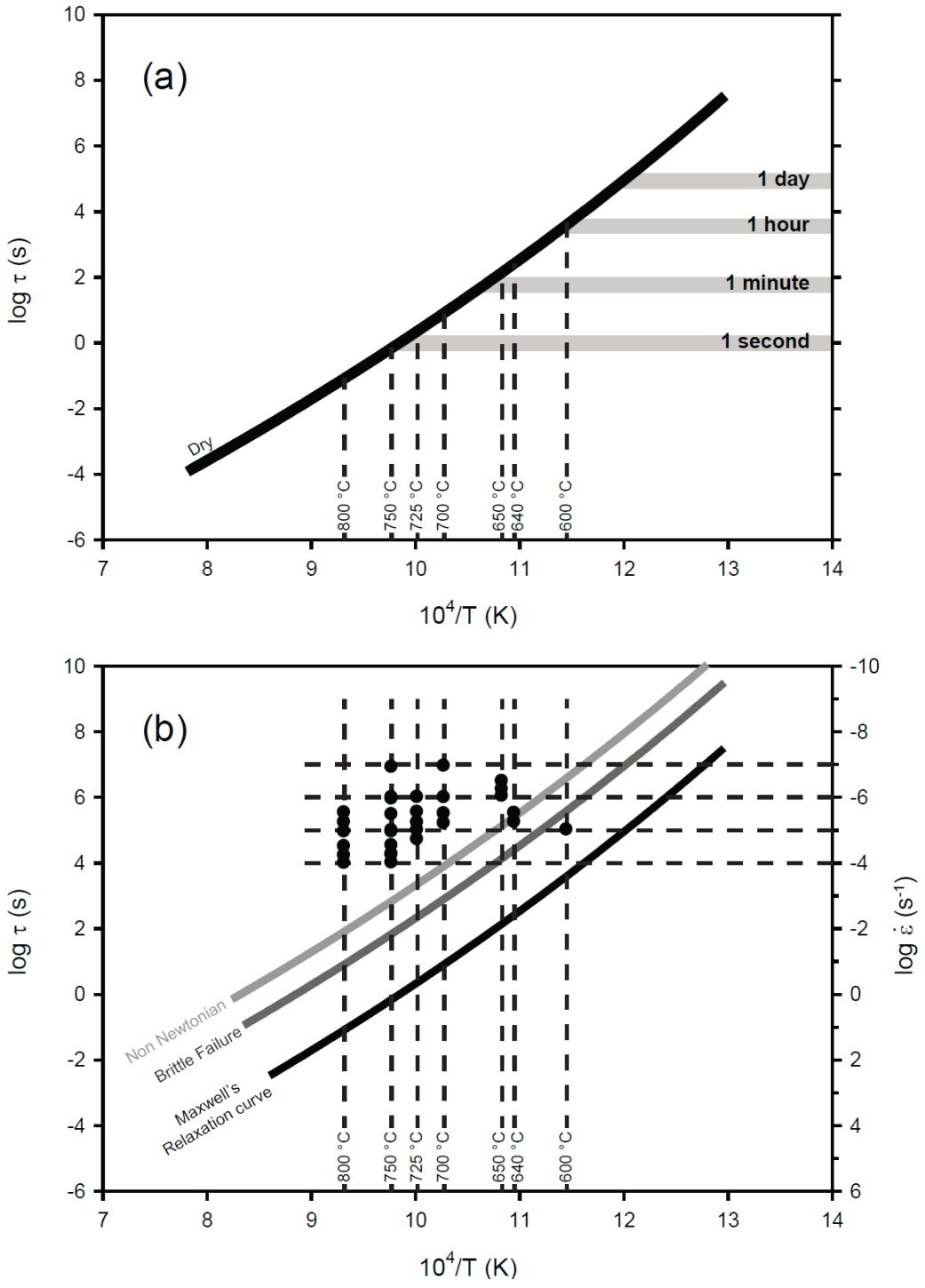

Figure 3

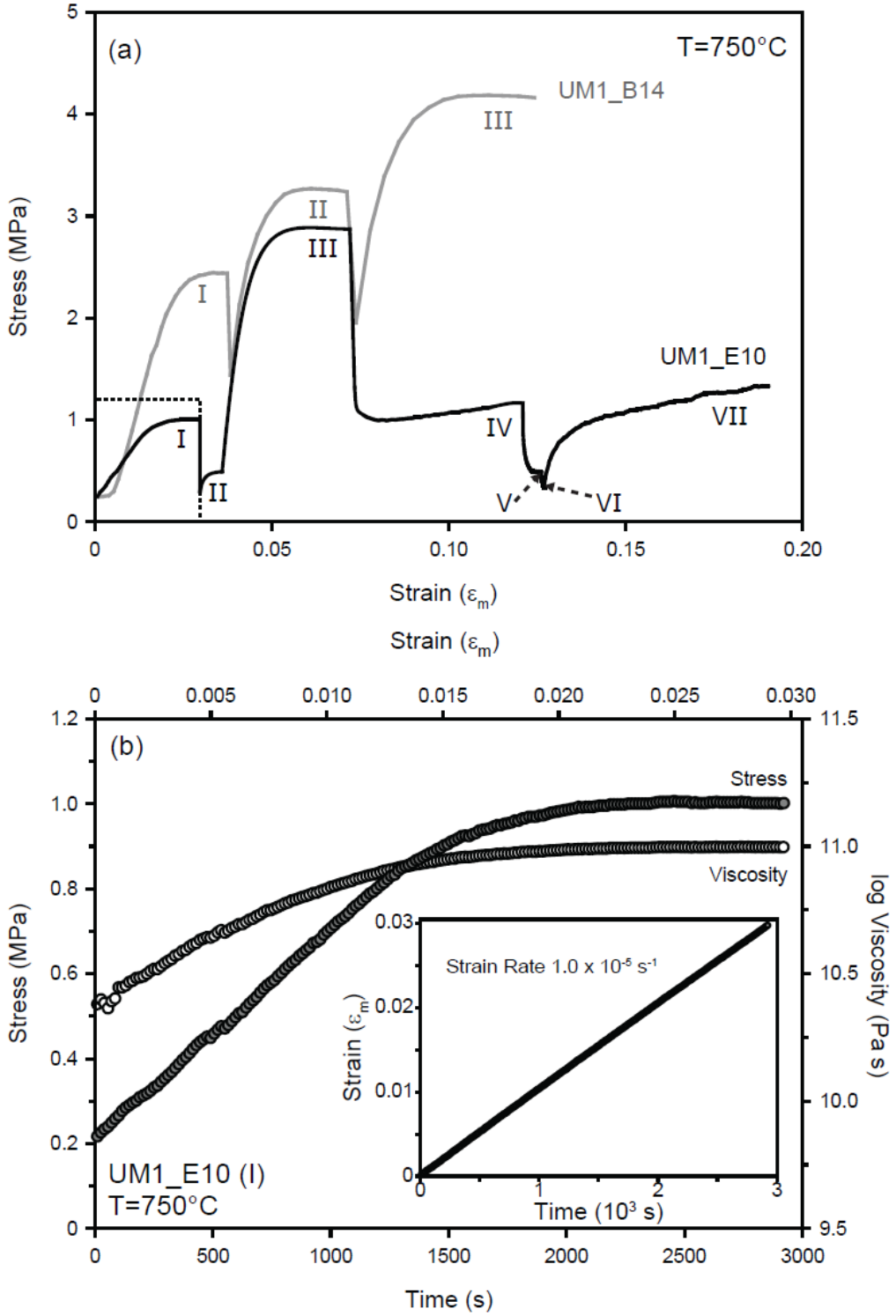

Figure 4

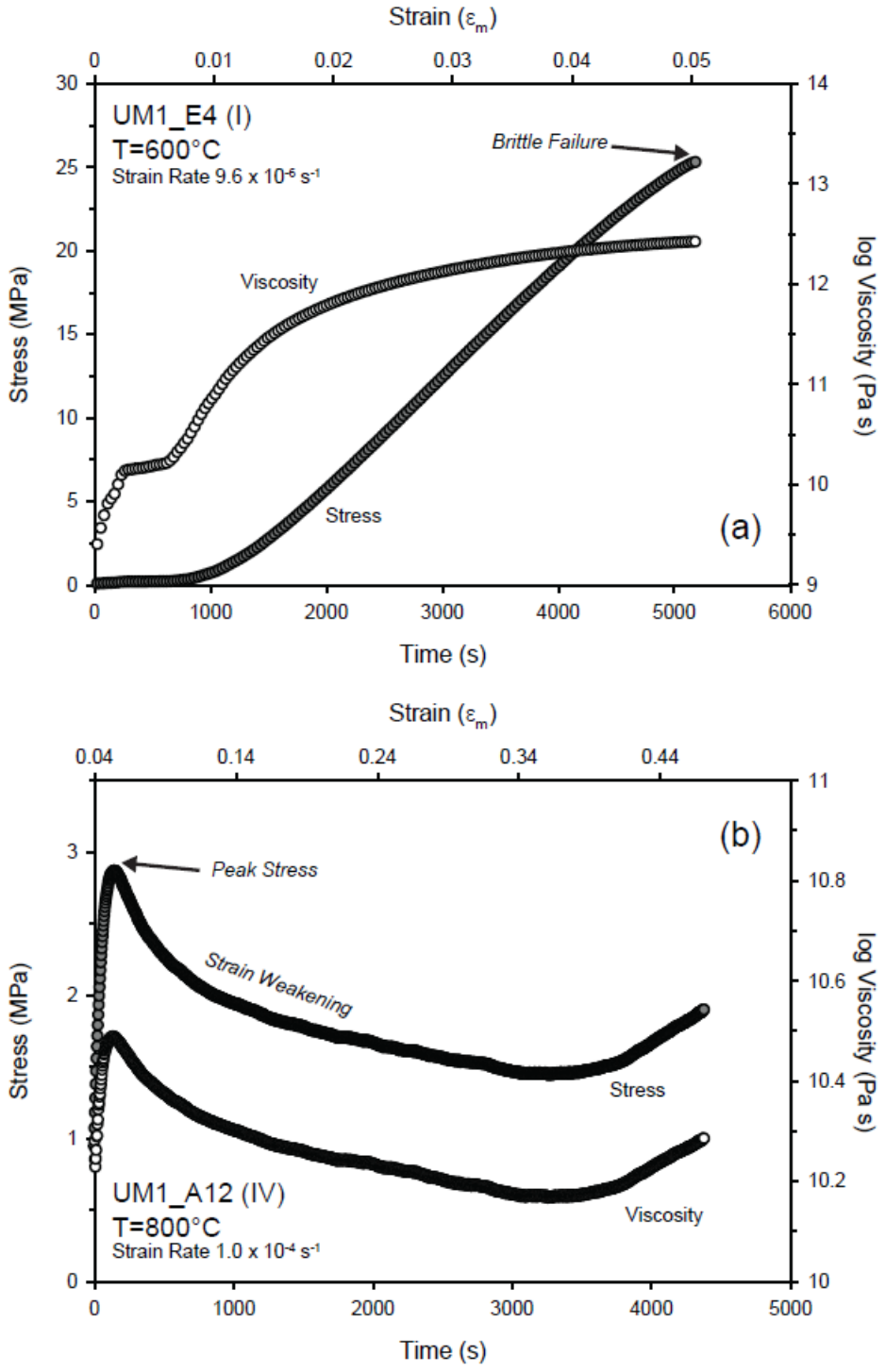

Figure 5

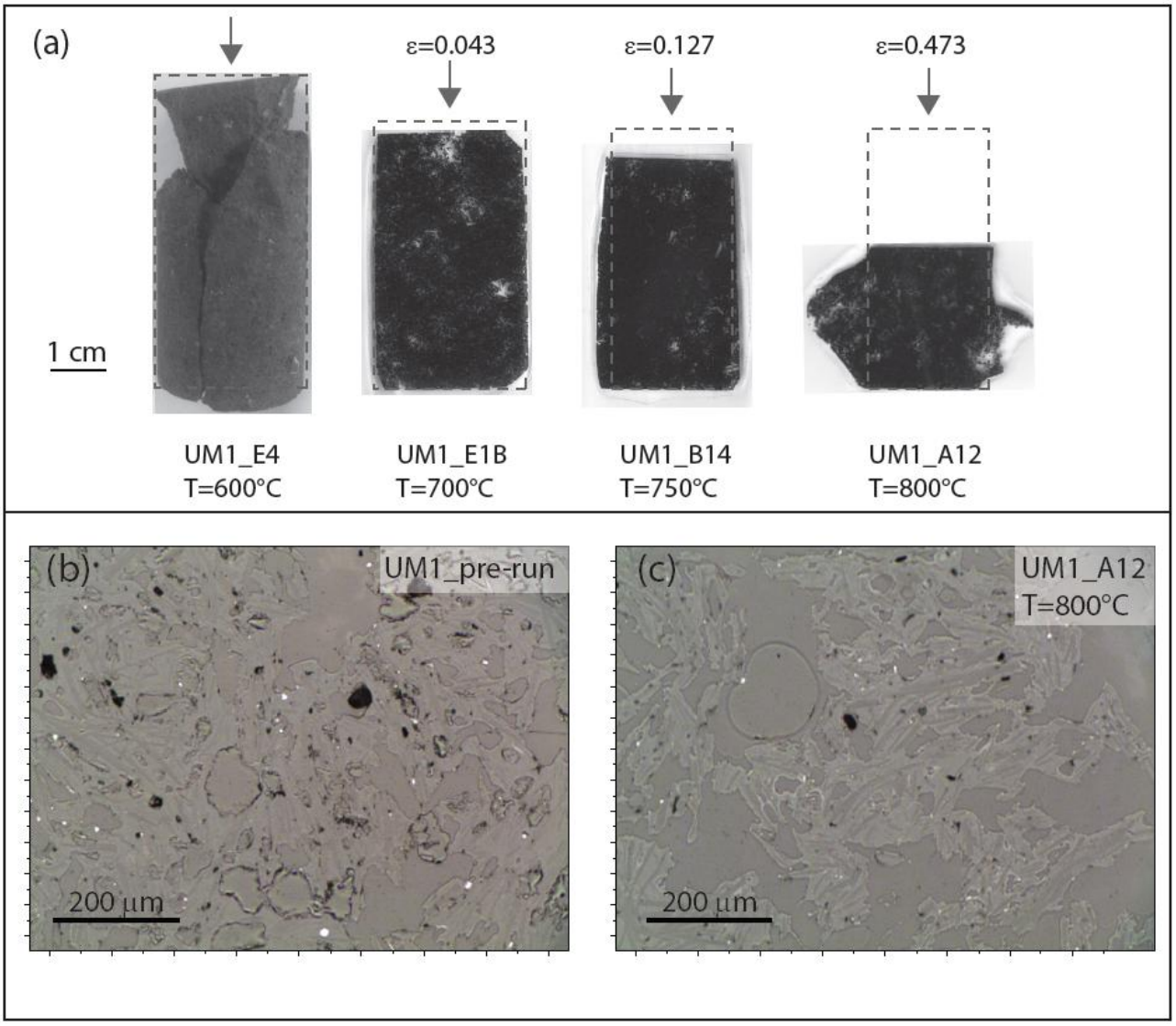

Figure 6

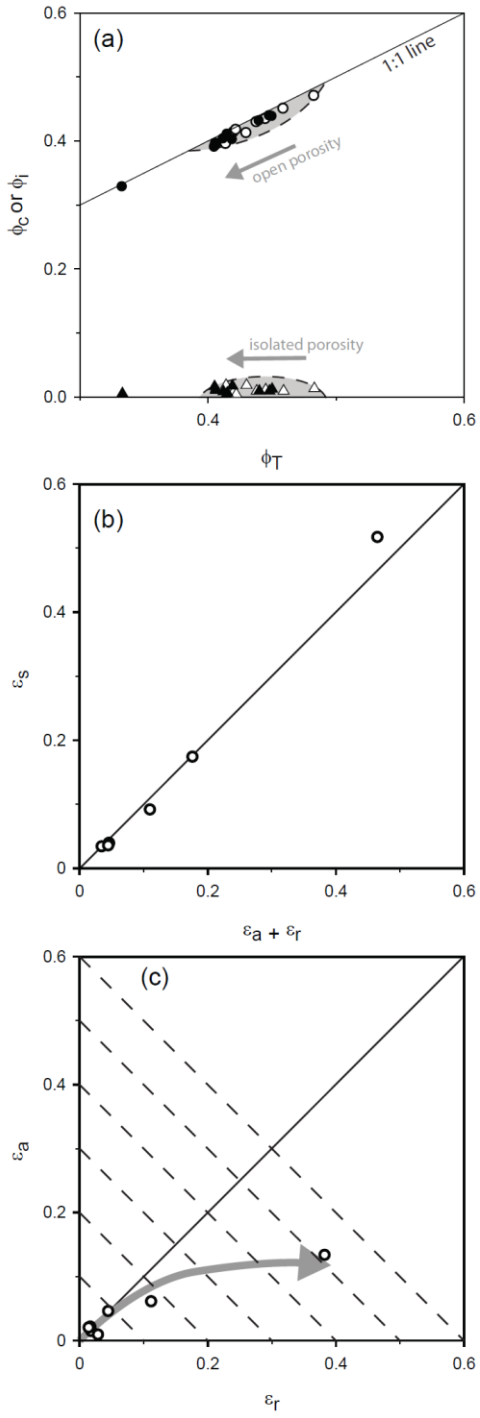

Figure 7

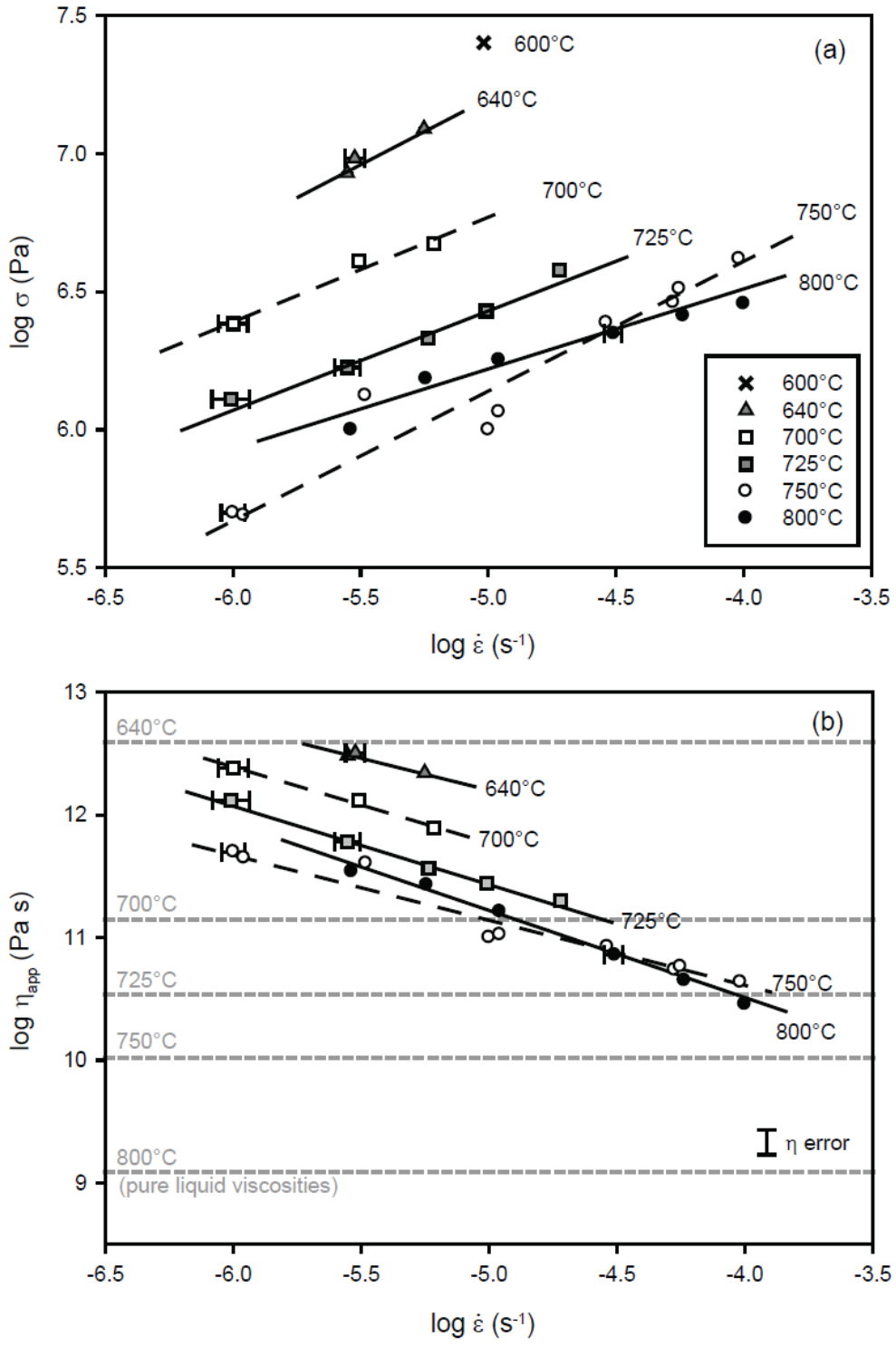

Figure 8

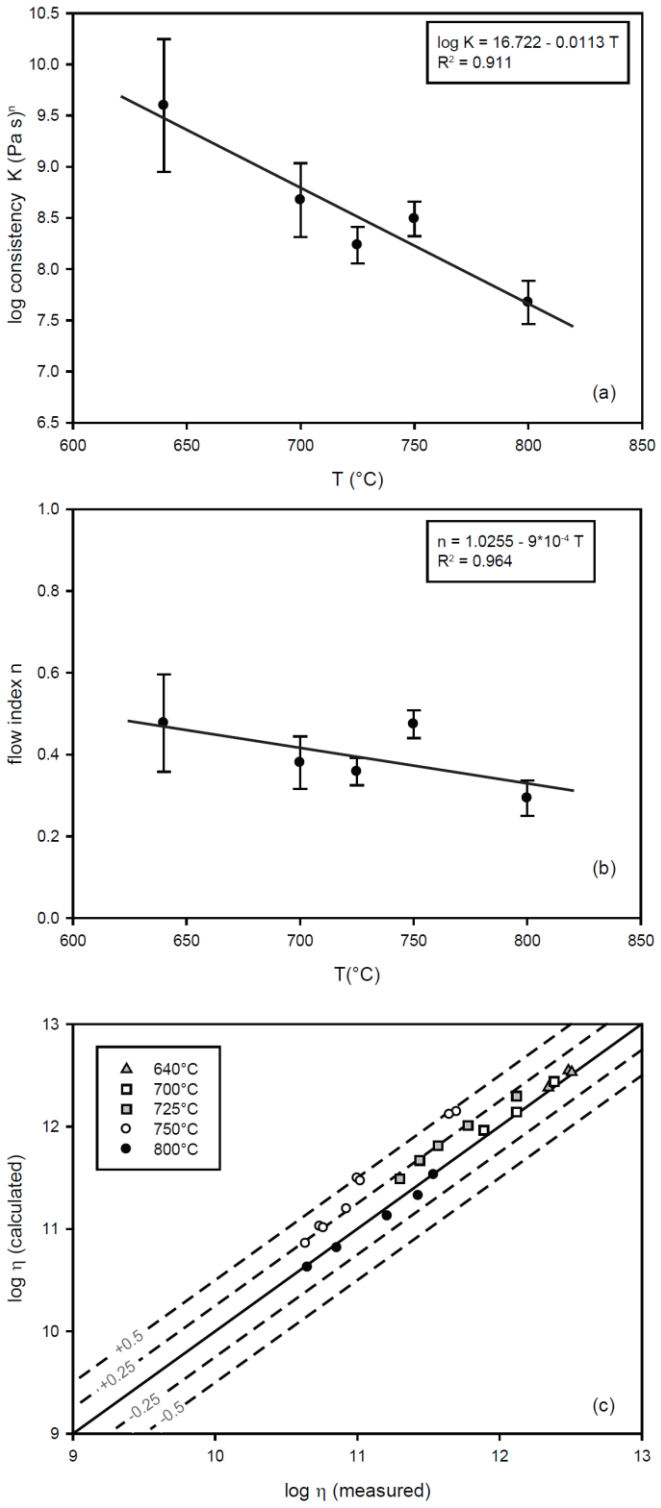

Figure 9